Numerical simulation framework for radio wave soil treatment for pathogen suppression

Sturm, G. S.J.; van der Wurff, A.; Linnenbank, S.; Bonnet, J.; Koppert, A.

DOI
10.1016/j.compag.2023.107992

Publication date
2023

Document Version
Final published version

Published in
Computers and Electronics in Agriculture

Computers and Electronics in Agriculture 211 (2023) 107992

Contents lists available at ScienceDirect

Computers and Electronics in Agriculture

journal homepage: www.elsevier.com/locate/compag

Numerical simulation framework for radio wave soil treatment for pathogen suppression

G.S.J. Sturm [a,*], A. van der Wurff [b], S. Linnenbank [c], J. Bonnet [d], A. Koppert [c]

[a] Process & Energy department, Delft University of Technology, Leeghwaterstraat 39, 2628 CB Delft, the Netherlands
[b] Groen Agro Control, Distributieweg 1, 2645 EG Delfgauw, the Netherlands
[c] Koppert Machines B.V., Vlotlaan 616, 2681 TX Monster, the Netherlands
[d] Stichting Control in Food & Flowers, Distributieweg 1, 2645 EG Delfgauw, the Netherlands

ARTICLE INFO

Keywords:
Pathogen suppression
Radio wave treatment
Numerical simulation

ABSTRACT

Thermal pathogen suppression in glasshouse horticulture by treatment with steam generated through combustion of fossil fuel will become progressively less desirable. Radio wave treatment could be an alternative. It has several advantages, the most notable is that it generates heat where it is needed in soil, so that it avoids heat losses and long process duration associated with heat transport. Radio wave treatment is a more dynamic and more complex process though, therefore more advanced development tools are needed to apply it effectively. To this end, this study describes the development of a framework for numerical simulation of this process to aid in the development of the radio wave treatment process. The modeling framework is Comsol Multiphysics in combination with Matlab, and the computational requirements are constrained to workstation grade hardware. Simulation results are presented to demonstrate the simulation.

1. Introduction

Presently steam treatment is being used for pathogen suppression in glasshouse horticulture. This is an energy and labor intensive process. In particular, regarding the latter aspect, it involves combustion of fossil fuels, which is undesirable due to the CO_2 emissions that are entailed. In view of these drawbacks, an alternative would be much desired. The context of this study is one such alternative. Specifically, treatment of soil with a radio frequency field, to heat the soil and thereby suppress pathogens. The primary system considered herein is the Agritron vehicle (Fig. 1) developed by Koppert Machines B.V., though the approach of this study can be generalized for similar applications. The Agritron is a tracked vehicle with a powerful radio frequency source that directs electromagnetic energy into the soil in an open ground horticulture context. In the soil, this energy is dissipated into heat, which causes suppression of pathogens. The vehicle directs a maximum of 100 kW of radio wave energy at a frequency of 915 MHz through an antenna into the soil that the vehicle rides over. The prototype treats a path of 1.2 m width; its operation is illustrated by the thermogram included in Fig. 1 (acquired with a FLIR A655sc thermal camera) that shows the heated track behind the vehicle. Video footage of an earlier prototype can be found online (Koppert Machines, 2014).

In comparison to current steam treatment practices, radio wave treatment has compelling attributes. In principle, it can be automated to reduce the labor requirement. It could potentially accommodate renewable electrical energy sources. It may also allow for more selective application of energy to soil, since at any instance only a relatively small amount of soil is treated, as opposed to a large surface bed that is treated in the case of steam treatment. Despite the compelling features, there are also considerable challenges. It involves complex and expensive custom-built equipment. Furthermore, the physical and biological processes that are involved with the treatment processes are more intricate. A plain trial and error approach would therefore be difficult to sustain.

To support the development of this treatment process, a computer simulation would be helpful to manage the complexities in an inexpensive and flexible manner. The goal of this present study is therefore to develop a framework for numerical simulation of radio wave treatment of horticulture soil. At present, there is little experimental data on this treatment process, especially with respect to the particular frequency band that is employed. Consequently, it would be problematic to validate the model, or to establish directions to guide its development towards. Accordingly, it is decided not to develop a model for a particular use case, but instead to develop a framework that maintains flexibility. As a body of practical and experimental experience on the process will materialize over time, this will allow subsequent iteration of

* Corresponding author.
E-mail address: info@guidosturm.nl (G.S.J. Sturm).

https://doi.org/10.1016/j.compag.2023.107992
Received 22 September 2022; Received in revised form 9 June 2023; Accepted 11 June 2023
Available online 13 July 2023

Appendix A List of Symbols

$\mathbf{B}$	magnetic flux vector
c	diffusion coefficient in PDE interface
c_0	speed of light in vacuum
C_n	function coefficients for coefficients numbered 0 to 7
$C_{p,a}$	specific heat of air
$C_{p,s}$	dry specific heat of solids in soil
$C_{p,sl}$	specific heat of solids and liquids in soil
$C_{p,wl}$	specific heat of liquid water
$C_{p,wv}$	specific heat of water vapor
d_a	damping or mass coefficient in PDE interface
$\mathbf{E}$	electric field vector component of the radio wave field
$\partial_t H_{s,sl,cc}$	enthalpy rate of change due to advection of temperature gradient
$\partial_t H_{s,sl,dc}$	enthalpy rate of change due to liquid water diffusion
$\partial_t H_{s,sl,hc}$	enthalpy rate of change due to thermal conduction
E_a	activation energy
f	source term in PDE interface
f	spatial volume fraction
f_A	function of Antoine equation that relates vapor pressure of water to temperature
f_D	function that relates diffusivity of moisture in soil to its moisture content
f_ε	function of humidity variation of Debye dielectric model parameters
g	gravitational acceleration
Gr	Grashof number
$\mathbf{H}$	magnetic field vector component of the radio wave field
$h_{n,m}$	mass transfer coefficient for natural convection
$h_{n,T}$	heat transfer coefficient for natural convection
$H_{s,sl}$	sensible enthalpy of liquid and solid part of soil
$H_{s,av}$	sensible enthalpy of water vapor and air in soil
$H_{v,0}$ H_v	enthalpy of vaporization of water
i	imaginary unit
ISM	Freiquency bands available for Industrial, Scientific, and Medical purposes.
j	species number
k	permeability for Darcy flow
k_0	vacuum wavenumber
$k(T)$	temperature dependent rate constant of pathogen inactivation kinetics
$k_{T_{ref}}$	rate constant of pathogen inactivation kinetics at reference temperature
L	characteristic length for natural convection
L_s	length scale related to surface evaporation boundary condition
M_a	molecular weight of air
M_w	molecular weight of water
$\frac{m_w}{m_t}$	mass ratio of humidity in soil to the total soil mass
N	pathogen population number
n	molar bulk density of a fluid in soil
$\overline{n}$	vector orthogonal to surface
n_a	molaxr bulk density of air in soil
N_L	pathogen population number on logarithmic scale
Nu	Nusselt number
n_{wl}	molar bulk density of liquid water in soil
n_{wv}	molar bulk density of water vapor in soil
p	pressure
$\widetilde{p}$	pressure with respect to ambient pressure
p_0	ambient pressure
PDE	partial differential equation
Pr	Prandtl number
p_v	vapor pressure of water
Q_{RF}	electxromagnetic heat generation
Q_v	heat of evaporation
$Q_{v,bc}$	heat of evaporation to surroundings in vicinity of soil surface
$Q_{\Delta T}$	sensible heat transfer
R	gas constant
Ra	Rayleigh number
RF	radio frequency
r_v	rate of evaporation
$r_{v,bc}$	heat of evaporation in vicinity of soil surface
Sc	Schmidt number
Sh	Sherwood number
T	temperature
t	time
T_{amb}	ambient temperature
T_{av}	temperature of gas and vapor
$T_{H_{v,0}}$	reference temperature for enthalpy of vaporization of water
T_{sl}	temperature of solid and liquid
T_{ref}	reference temperature for pathogen inactivation kinetics
u_0	vehicle velocity
$\overline{u}_{av}$	gas and vapor velocity in soil, including imposed advection
$\overline{u}_{Darcy}$	flow in porous medium according to Darcy's Law, not including imposed advection
u_w	flow velocity in direction of coordinate w
V	arbitrary variable
$\mathbf{V}$	arbitrary vector variable
$\widehat{V}$	smoothed arbitrary variable, indicated by caret
$V(t)$	function of separated variable t
w	coordinate perpendicular to boundary plane
WR975	waveguide, rectangular of 9.75″ width
$W(w)$	function of separated variable w
α	thermal diffusivity of ambient air
α	conservative flux convection coefficient in PDE interface
α_{combi}	combined diffusivity
α_p	diffusivity of gas and vapor pressure in soil
α_s	smoothing parameter
α_v	diffusivity of water vapor in air
α_w	diffusivity of moisture in soil
β	thermal expansion coefficient of ambient air
β	convection coefficient in PDE interface
β_v	relaxation length
γ_p	inverse length scale related to pressure boundary condition in soil
γ_s	inverse length scale related to surface evaporation boundary condition
ΔT	characteristic temperature difference between soil surface and ambient air
ε	dielectric permittivity
ε'	real part of the complex relative permittivity
ε''	imaginary part of the complex relative permittivity
ε_∞	dielectric permittivity at infinite frequency
ε_0	permittivity of vacuum
ε_e	dielectric permittivity of environment species
ε_i	dielectric permittivity of inclusion
ε_j	dielectric permittivity of j-th species
ε_{eff}	effective dielectric permittivity
ε_r	complex relative dielectric permittivity
ε_s	dielectric permittivity at zero frequency
κ	thermal conductivity of soil
κ	thermal conductivity of ambient air
κ_{av}	thermal conductivity of air in porous volume of soil
μ	dynamic viscosity
μ	dynamic viscosity of ambient air
μ_0	magnetic permeability of vacuum

μ_r	complex relative magnetic permeability	τ	relaxation time constant of dielectric polarization
ρ	density of ambient air	τ_v	relaxation time constant
ρ_s	dry density of solids in soil	φ	relative porous volume
ρ_{wl}	density of liquid water	ω	angular frequency of the radio wave field
σ	electric conductivity	ω_{bc}	characteristic radial frequency of process dynamics

the model. In effect, we propose to develop the practical and experimental knowledge in parallel with supporting computer models. The simulation framework that is presented herein hence amounts to the first step on the simulation side, and is to be improved upon at later stages.

This article continues in Section 2 with an overview of the context of the development, and the objectives for the numerical model. Section 3 presents a general overview of the model, while Sections 4 to 7 discuss the model descriptions of the individual sub-processes. Section 8 demonstrates and evaluates the model with simulation results, and is followed by a concluding section.

2. Context and objectives for model development

The objective for the simulation framework is to facilitate evaluation of several aspects relevant to the context of radio wave treatment of soil. These are: the dynamic nature of the radio wave treatment process; the effect of the operating frequency; the potential occurrence of intricate biological mechanisms that relate in a complex manner to temperature development; and the integration with wider energy supply systems.

2.1. Rapid treatment process, more parameters

Steam treatment (Dabbene, et al., 2003), the method for pathogen suppression that radio wave treatment intends to replace, is outlined as follows. First a large sheet is manually placed over the soil, and weights are placed around the edges to contain the gaseous volume under the sheet. Then, superheated steam is injected under the sheet. Optionally, porous vacuum lines are installed in the soil to provide suction to draw heat into the soil. Over a period of several hours the soil temperature will rise sufficiently and down to a sufficient depth to suppress or eliminate pathogens that damage crops. For steam treatment, the treatment parameters essentially are limited to the duration and the suction pressure applied to porous tubing in the soil.

Radio wave treatment, in contrast, involves many more factors. Parameters to consider are: the much shorter duration of the exposure; the desired peak temperature; the desired rate of temperature rise; the vehicle velocity; the radio wave power; and the potential implementation of demand response integration with the electricity network as will be explained in the next section. Optimum treatment settings are to be determined for each case that is defined by: soil type and composition; type and number of pathogens that are present; and the crop that is cultivated. This increased complexity makes it more difficult to find an optimum treatment solution via practical trials alone.

2.2. Operating frequency selection

Much of the difficulty stems from the introduction of radio wave heating equipment into a horticulture environment. In particular because it concerns less accessible custom-built 915 MHz equipment. For heating applications, several frequency bands are available that are known as ISM (Industrial, Scientific and Medical) bands (ITU, 2020). For other ISM bands, equipment is more readily available, most notably domestic microwave ovens for the 2450 MHz band. Hence studies would understandably gravitate towards those other frequencies. A review by Nelson (1996) reports on several works on the application of electromagnetic fields for soil disinfestation dating back to the 1970s. In it, the author includes a few studies that use radio frequency fields in either the 27 MHz or the 40 MHz ISM bands. Aside from these, all other studies use the 2450 MHz band, many by means of domestic microwave ovens. What Nelson concludes is that applicability of microwave energy is restricted due to the limited depth to which the microwave field can penetrate into soil, in addition to the high energy demand. One of the studies mentioned is the work by Ferriss (1984), who concludes that microwave energy is indeed effective, though only on a small scale.

Research has been ongoing. Rasing and Jansen (2007) demonstrate the effectiveness of electromagnetic heating on potting soil and agricultural substrates. They report on both a 27 MHz and a 2450 MHz source. In a later work (Rasing & Jansen, 2010), they report on the feasibility of a variety alternatives for steam treatment, including the Agritron system. In a development similar to the scope of the Agritron,

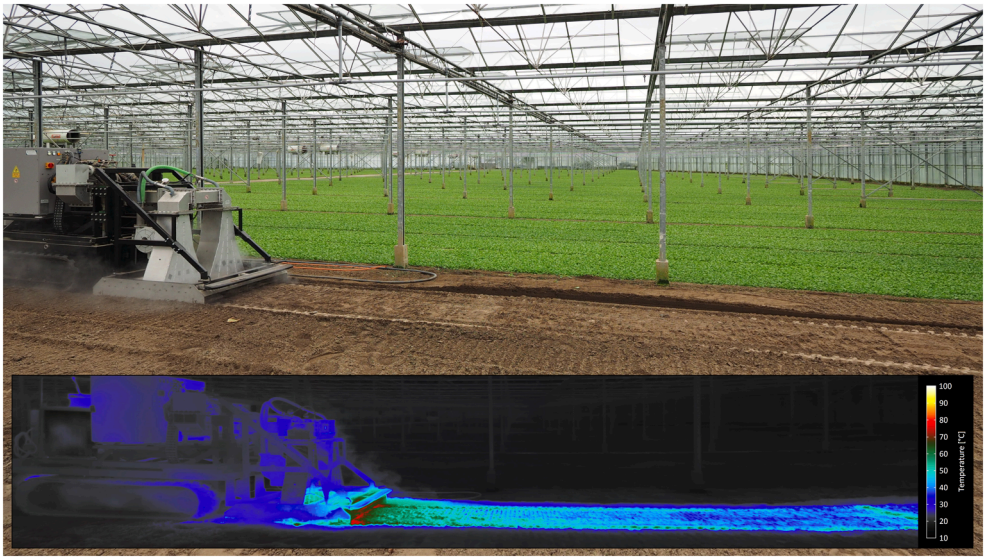

Fig. 1. Agritron prototype in operation; thermogram captured with FLIR A655sc with 24.6 mm T197922 lens.

Brodie and co-workers (2012) (2015) (2020) show the effectiveness and operational flexibility of 2450 MHz systems. Their studies involve irradiation through antennas downward onto soil, both in a configuration with a column of soil exposed by a static generator, and in a different configuration with a mobile generator that is drawn over the soil surface in a field.

The choice for a particular frequency in many cases is likely expediently decided upon based on availability and cost of equipment. The selection in particular cases can be entirely valid, though it must be noted that the frequency band impacts the effectiveness of the treatment. The domestic microwave ovens that are often used for research purposes are not designed specifically for the purpose of soil disinfestation, rather their purpose is to prepare food. Likewise, the 2450 MHz frequency band that is used in these devices has been intended primarily for food preparation. The power output of these devices is limited to around a kilowatt, though industrial generators that provide up to 6 kW are also available. For small scale processes this may suffice, as does the efficiency of 60–70 % (Radoiu, 2011) (Meredith, 1998) that is typically offered by the magnetron tubes at this frequency. In contrast, thermal treatment of large volumes of soil, be it in open ground horticulture or batch-wise substrate volumes is much more energy-intensive. This directs the design of equipment to 915 MHz water–cooled magnetrons that have a much larger output of 100 kW and better efficiency of 80–90 % (Radoiu, 2011) (Meredith, 1998). In addition, the longer wavelength of 915 MHz systems allows for deeper treatment of soil. Specifically, the depth of penetration scales by approximation with the ratio of the frequencies. Thus, at the longer wavelength of a 915 MHz radio wave field, the treatment can be expected to be about three times deeper than at 2450 MHz. This also explains the restricted treatment volume reported in aforementioned prior studies (Nelson, 1996) (Ferriss, 1984). It has to be noted though, that a rule of thumb argument that states that 915 MHz is always preferable would not be well-considered. For example, the aforementioned studies by Brodie and co-workers aim for a shallow treatment. Consequently, in their case the higher operating frequency is preferred.

2.3. Intricate biological processes

Another aspect that may determine if radio wave heating is suitable, and if this is the case, what frequency is preferred, is the expected mechanism of action. At present, much remains unknown about the exact mechanism by which pathogens or crops are affected by radio wave fields. It is known, however, that intricate biological effects can be at play. Ample literature is available on the effects of thermal treatment of soil, on pathogens in soil, and the ability of soil to support crops and organisms. A comprehensive source in this context primarily on the topic of soil solarization is the work edited by Katan and DeVay (1991a). They mention in one of their contributions (Katan & DeVay, 1991b) non-monotonic and interdependent interactions between soil and the organisms that it supports, for example the need to avoid “disturbing the biological balance” and the risk of “creating a ‘biological vacuum’ which may facilitate a rapid and severe reestablishment of reinfesting pathogens”. Some of their co-contributors (Griffin & Baker, 1991) (Chen, et al., 1991) refer to such processes as “the boomerang effect”, the general case in which a treatment creates an opportunity for pathogens to reestablish and reinfest, which negates the desired effect of the treatment process. A different publication provides an example related specifically to steam treatment; Roux-Michollet et al. (2010) showcase a treatment in which the number of bacteria – fluorescent pseudomonads populations – increases considerably. It is hypothesized that the slow acting steam treatment allows time for these bacteria to counteract the elevated temperature, and to subsequently quickly repopulate after temperature has dropped. A more rapid treatment may inhibit pathogen survival mechanisms such as spore formation or relocation. Aside from permitting time to deploy survival mechanisms, steam treatment might also release the water-soluble part of organic matter, which may benefit undesired organisms. This concerns bacteria in particular (Bollen, 1969), but may include certain species of fungi too, such as *Aspergillus fischeri*, *Penicillium luteum* and *P. baarnense* (Warcup, 1951). A more dynamic treatment method could avoid such occurrences, in particular when the maximum temperature is regulated below a pre-determined threshold at which organic matter is released. For steam treatment this could be difficult, because steam is invariantly at a boiling temperature of 100 °C. In contrast, for radio wave treatment there is more flexibility in the maximally applied temperature. The intricacy of interacting biological systems is further illustrated several examples included herein. The work of Abbey, et al. (2017) who investigate the treatment with microwave energy of vermicasts to increase the bioavailability of nutrients and induce plant growth enhancement. Miler & Kulus (2018) investigate the potential of microwave irradiation for mutation breeding of chrysanthemum. Mahdi, et al. (2021) study the effect of microwave radiation on fungi, bacteria and growth characteristics. Khan, et al. (2016) investigate the effect of microwave treatment to enhance wheat yield. These studies all employ a microwave field at 2450 MHz, and observe effects beyond a straightforward thermal effect of microwave exposure on pathogen inactivation. Consequently, despite the fact that the Agritron operates at a frequency that is close to but different from the 2450 MHz frequency that is used in these studies, it must be noted that a provision is desired in the modeling framework that allows more intricate biological effects like the ones mentioned here to be included in it, as well as to allow for a different operating frequency.

2.4. Integration into energy infrastructure

A final aspect that relates to the development of radio wave treatment of soil are the global environmental challenges. As the past restrictions of pesticides, fumigation agents or other chemical means of pest control were important incentives for the shift towards thermal treatment of soil with steam, a similar transition is likely to occur if progressively more restrictions on carbon dioxide emissions come into force. If renewable electrical power becomes the sole source of energy that is available for thermal treatment of soil, then radio wave heating is the straightforward design option. The main benefit is that it enables heat to be generated selectively in the location where it is actually needed, rather than being generated in a boiler and subsequently transferred by steam or another heat transfer agent, incurring losses in the process, and being applied non-selectively to a large volume of soil. Moreover, a fluctuating renewable source can in principle be accommodated by real-time coordinated adjustment of both the generation of radio wave power and the driving speed of the vehicle. In this manner, radio wave treatment of soil could serve a secondary purpose as a demand response application (Conchado & Linares, 2012) that is integrated with short term electricity markets, specifically the intraday market and imbalance market (Welle, 2016) (Agro Energy, 2017). As such, dynamic variation of electricity consumption could be used to take advantage of low short term electricity prices. Possibly radio wave treatment could even be used to directly control the imbalance between supply and demand on the electricity grid.

2.5. Objectives

To address these contextual aspects, the modeling framework would primarily have a physics and engineering focus. At this stage a high fidelity simulation is not called for, although this may change at a later stage. The following features would be desired,

- Flexibility to be adapted to particular treatment cases as an intermediate step in the development of optimum treatment procedures for such cases.
- Flexibility to be expanded with detailed biological process descriptions to evaluate the effects of these process variations on the treatment effectiveness via parametric studies.

- The possibility to evaluate and iterate the designs of the equipment for radio wave treatment via simulation as an intermediate step in the design process, i.e. to provide a "Virtual Agritron".
- The possibility to evaluate the effects of dynamic variation of the availability of renewable electrical energy sources.
- A sufficiently low computational requirement to run the simulation on workstation grade hardware.

3. Model overview

The model described herein is developed to simulate radio wave heating of soil for disinfestation purposes. It is primarily intended as a tool for engineering and design of both the equipment for radio wave treatment of soil and for the processes of soil treatment with radio wave energy. Consequently, the aim is to make the modelling approach accessible on workstation grade hardware, and therefore several measures are taken to reduce the computational requirements. Moreover, it is desired to use commercial software packages for numerical simulation. For this study, Comsol Multiphysics 5.5 (COMSOL AB, 2019) in combination with Matlab (The Mathworks, 2019) are selected. This combination has sufficient flexibility to allow progressive improvement of the modeling approach upon an initial framework. This section continues with an outline of the modeling methodology and the approach to reduce the computational requirements. It discusses: the model geometry; the manner in which the respective sub processes are handled; and the simulation steps including the arrangement for antenna motion.

3.1. Model geometry

In order to reduce the computational requirements and to generalize the approach, a simplified geometry is used instead of the particular design of the Agritron prototype. The radio wave heating system is represented by a horn antenna as described by R. Meredith (1998) that is directed downwards into a body of soil while moving over it, as is depicted in Fig. 2. The input dimensions of the horn are equal to a WR975 waveguide, which is in accordance with the 915 MHz operating frequency. The model geometry includes only one symmetry half to reduce the computational requirement. The modeled soil volume is 3 m long, 0.6 m wide, and 0.5 m deep; this amounts to one symmetry half.

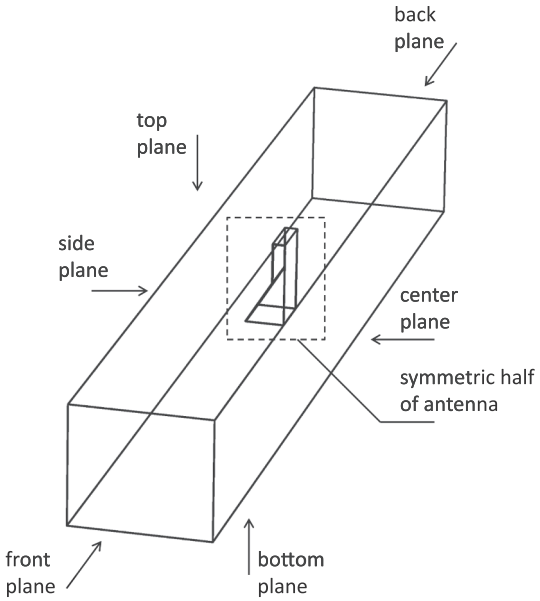

Fig. 2. Model geometry.

3.2. Sub-processes

The soil treatment process – depicted in Fig. 3 – is divided over four sub-processes: the electromagnetic process; the heat and mass transfer process; the pathogen inactivation; and crop growth. The first three processes are included in the simulation approach described herein.

The first is the electromagnetic process concerning the transmission of the radio wave field through the antenna into the soil and possibly also the surroundings. This process causes heat generation in the soil. In the simulation, an electromagnetic inlet port condition is imposed on the horn antenna; for simplicity no additional radio wave equipment is included in the simulation. Electromagnetic energy transmission is simulated through the antenna and into the soil. Partial scattering to the above ground surroundings is also included. Section 5 and 6 discuss the electromagnetics model and the dielectric model respectively.

The next sub-process is comprised of the transport phenomena of heat and mass transfer in the simulated soil volume. In general, coupled diffusion of moisture, heat, and vapor pressure through a porous medium may combine into more convoluted physical interactions (Henry, 1948). In our case, soil is moist but not saturated with water; the soil zone that is being heated lies above the water table (Bear, 1972). This soil is porous, and pressure in its pore volume is therefore not due to hydraulic pressure of liquid water, but due to atmospheric pressure and – at elevated temperature – due to the vapor pressure of water. Heat transfer occurs through several mechanisms. There is thermal conduction in soil, but also convection of heat though diffusion of liquid water. Moreover, since temperatures in excess of 70 °C are reached, vapor is generated which induces flow of air and water vapor present in soil. This subsequently causes additional convective heat transfer with this gas and vapor flow. In the simulation this flow is represented by Darcy's law (King Hubbert, 1956); in effect it represents internal "steam" heating in the soil that is driven by vapor pressure caused by moisture heated by the radio wave field. The physical phenomena are mutually coupled, i.e. the electromagnetic field causes temperature and pressure variations in soil that drive the transport phenomena, but the resulting variations of temperature and humidity alter the electromagnetic properties of soil so there is a feedback effect back towards the electromagnetic interactions, as is indicated in Fig. 3. Section 4 discusses the simulation of transport phenomena in this study.

The final sub-process that is considered herein are the kinetics of pathogen inactivation in response to radio wave heating. In contrast to the two aforementioned sub-processes, pathogen inactivation is not simulated in Comsol Multiphysics, instead the temperature development is exported into Matlab to calculate the response in pathogen numbers by means of an Arrhenius model. The focus of this present study is on the physical processes, i.e. the first two sub-processes of Fig. 3. A simple pathogen inactivation model is nevertheless included to explore the interaction of the biological processes with the physical processes. Section 7 provides more detail on the pathogen inactivation model.

3.3. Motion through advection and simulation steps

The overall modeling approach is comprised of three steps:

1. For physical interactions that involve the radio wave interactions a three-dimensional stationary simulation is used.
2. For physical interactions that do not involve the radio wave field and occur over longer time scales, specifically time scales of minutes and hours after the antenna has passed, a two-dimensional dynamic simulation is used.
3. Finally, biological interactions are simulated from the combined results of the two prior steps that consider physical interactions.

In the first step that uses the three-dimensional modeling approach (geometry shown in Fig. 2) the horn is not moving over the soil, instead the horn is stationary while an advection velocity u_0 is imposed on the

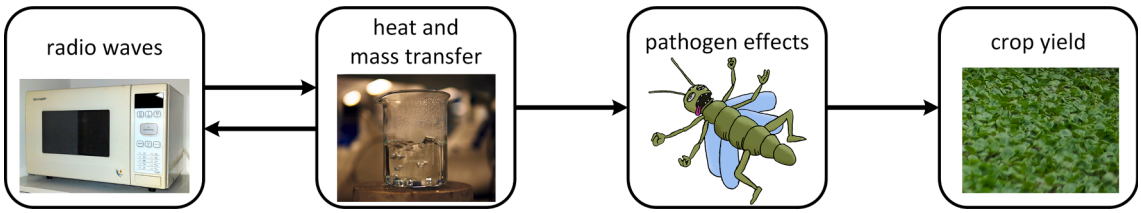

Fig. 3. Sub-processes of radio wave treatment.

soil domain. In short, the soil is made to move in the simulation rather than the horn. This arrangement avoids the need for a time dependent simulation with a variable geometry. Furthermore, it also allows for frugal meshing of the model geometry, as a fine mesh can be concentrated in the zone directly under the horn while for other parts of the geometry a courser mesh suffices. In the step that follows, a two-dimensional simulation is performed over longer time durations in a cross section of soil that is perpendicular to the direction of motion. The antenna is not included here, because it will have long since moved away. Moreover, gradients along the direction of motion will be relatively small, which justifies a two-dimensional modeling approach. The transition between the three–dimensional and two-dimensional approaches is performed via interpolation functionality available in Comsol Multiphysics. As mentioned in the introduction to Section 3 and in Section 3.2, in the third step the temperature data is finally exported into a Matlab environment to compute the pathogen response.

4. Transport phenomena in soil

This section describes the model for the coupled transport phenomena of heat and moisture in soil. These phenomena are not represented by the default physics description in the software package. A custom model description is therefore developed. An overview of key aspects related to the transport phenomena model is provided below. In particular: the relevant transport phenomena that occur are introduced; the manner in which moisture transfer between liquid phase and vapor phase inside the soil volume is handled; the state variables are introduced; and finally the method for maintaining numerical stability of the simulation is described. Following this overview subsequent sections provide a detailed discussion of the modeling methodology of transport phenomena: Section 4.1 discusses medium properties; Section 4.2 details the coupling between gas/vapor and liquid/solid phases; Section 4.3 presents the model equations for transport phenomena; finally Section 4.4 discusses the boundary conditions for transport phenomena.

The transport phenomena in soil comprise of: 1) flow induced by pressure variations in gas and vapor, which is expressed by Darcy's law; 2) diffusion of water vapor though air present in the porous soil volume; 3) diffusion of liquid water in soil; 4) thermal conduction in soil; 5) convective heat transfer by the flowing media; and 6) the virtual transport of heat through imposed advection that represents the relative motion of soil under the horn antenna.

Inside the soil volume, moisture is transferred between liquid and vapor phase. This is accommodated by simulating two coinciding domains of different phase in the soil volume. The first domain describes the gas and vapor phases, comprising of air and evaporated moisture. The second domain describes solid soil and liquid water. The state of the former is defined by gas/vapor temperature (T_{av}), gas/vapor pressure (p), and molar bulk density of water vapor (n_{wv}). The state of the latter domain is defined by the solid/liquid temperature (T_{sl}), and molar bulk density of liquid water (n_{wl}). Note that the two volumetric bulk densities are expressed in mol/m^3 over the total soil volume, i.e. not just over a porous or non-porous/condensed volume fraction. As most of the thermal mass is contained in the solid/liquid phase domain, for those cases in which a temperature T is considered that does not relate to a specific phase domain, this temperature will be approximated by the one of the solid/liquid domain, i.e. $T \approx T_{sl}$.

As it turned out, the mesh size of the model could not be made sufficiently fine to suppress Runge's oscillations, i.e. instabilities due to advection of discontinuities at transitions between mesh elements. The requirement to run the simulation on workstation grade hardware directed towards a different approach to suppress these numerical artifacts. A diffusive smoothing parameter $\alpha_s = 6.25{\cdot}10^{-6}$ m^2 term was applied according to the following equation,

$$\alpha_s \nabla^2 \widehat{V} + \widehat{V} = V \tag{1}$$

here V represents the particular variable and the caret indicates smoothing. Despite the fact that this could be considered an alteration to the physics representation, the diffusive effect is small enough for the purposes of this model. Specifically, the diffusive smoothing parameter was progressively reduced in subsequent trial simulations until the simulation was close to instability. At that instance the characteristic length of this effect was determined to be $\sqrt{6.25 \bullet 10^{-6}} = 2.5 \bullet 10^{-3}$ meter. This was judged to be acceptable in relation to the larger length scales over which the treatment process is evaluated.

4.1. Medium properties

This section introduces many new model parameters and variables. Appendix A lists their symbols and meaning in combination with all other parameters, variables, and other abbreviations in this study.

A simplified viscosity (μ) model is implemented for the gas/vapor phase of a constant value of 15 μPa·s. The Engineering Toolbox provides a value of 17 μPa·s for air (2003b), and provides a value of 11 to 12 μPa·s for steam or water vapor (2004c). The value of 15 μPa·s is a suitable approximation to lump the respective values together. From Bear (1972) representative values were obtained for porosity and permeability; the porous volume available to air and vapor (φ) was set at 0.05, and permeability (k) at 10^{-9} cm^2. These values correspond to fine sand. Data from Mills (1999) for thermophysical properties of soil was adapted to bring it in accordance with the aforementioned data from Bear for dry and wet soil at 0 resp. 300 kg water per cubic meter of soil. The values for the thermophysical properties are as follows. Density: dry 1500 kg/m^3, wet 1800 kg/m^3 (300 kg of moisture per m^3 of soil); specific heat: dry 1900 J/kgK, wet 2280 J/kgK; and thermal conductivity (κ): dry 1 W/mK, wet 2 W/mK. In the model calculations, soil and moisture are handled separately; symbols for soil (excluding water) density and specific heat are resp. ρ_s and $C_{p,s}$. The thermal conductivity is linearly interpolated between the two aforementioned values.

The thermophysical properties of water, water vapor, and air as they are used herein are listed as follows. Specific heat of liquid water ($C_{p,wl}$) is constant at 4180 J/(kg·K) (The Engineering Toolbox, 2003d); specific heat of water vapor ($C_{p,wv}$) is constant at 1870 J/(kg·K) (2005); the enthalpy of vaporization of water ($H_{v,0}$) is 2477 kJ/kg (2010) at a reference temperature of 10 °C ($T_{H_{v,0}}$) and varies linearly with temperature to account for the accumulating variation in sensible heat between liquid and vapor as temperature increases; the density of liquid water (ρ_{wl}) is 1000 kg/m^3 (2003d); the specific heat of air ($C_{p,a}$) is constant at 1006 J/(kg·K) (2004b); molecular weight of air (M_a) is 29 g/mol (2004a); molecular weight of water (M_w) is 18 g/mol. The thermal conductivity of air is $\kappa_{av} = 24.35$ mW/mK (2003c). The diffusivity of

water vapor in air is $\alpha_v = 0.28$ cm^2/s (Wikipedia, 2019).

The diffusivity of liquid water in soil is too variable with the moisture content to impose a constant or linearly varying value. Table 1 presents the values from Staple (1965) (in part extrapolated) for the diffusivity (α_w) of moisture in soil. A function is defined from these values that relates the diffusivity expressed in m^2/s to liquid molar bulk density (n_{wl}) expressed in mol/m^3,

$$\alpha_w = f_D(n_{wl}M_w/\rho_{wl}) \tag{2}$$

Another variable that cannot be represented by a constant or a linear relation is the vapor pressure of water (p_v). The Antione equation from the NIST webbook (2018) is used with the 71 – 100 °C fit, as this is the range where vapor and air flow driven by a pressure differential is strongest.

$$log_{10}(p_v) = 10.08354 - \frac{1663.125}{T - 45.622} \tag{3}$$

In this equation, temperature (T) and vapor pressure (p_v) are expressed in K and Pa, and the Antoine equation is represented by a function $p_v = f_A(T)$.

4.2. Coupling between gas/vapor and liquid/solid phases

In principle, for a porous medium like soil, it can be assumed that the liquid and vapor phases of water are at thermal equilibrium throughout the soil due to the intimate contact between the two phases. However, if that were to be implemented in a simulation, then the stiff interaction between the respective sets of model equations makes finding a converged solution difficult. In order to facilitate convergence, a first order relaxation process is imposed between the two coinciding domains of different phase. The rate of this relaxation process is defined in terms of a characteristic relaxation length β_v that is converted to a time constant through division by the antenna velocity,

$$\tau_v = \beta_v/u_0 \tag{4}$$

The characteristic length β_v is set to 10 mm. A sequence of trial simulations has determined that this is close to the shortest length at which the simulation still converges. This characteristic length is sufficiently short to not impact the simulation results over length scales of interest in the scope of this study.

The rate at which moisture transfer between the respective solid/liquid and gas/vapor domains occurs is calculated as follows, Vapor pressure of equilibrium in soil is defined as,

$$p_v = f_A(T_{sl}) \tag{5}$$

The ideal gas law is used to calculate the molar bulk density of water vapor at equilibrium. The difference of the actual molar bulk densities of water vapor (n_{wv}) and the equilibrium value divided by the time constant determines the volumetric rate of moisture transfer between the solid/liquid domain and the gas/vapor domain due to evaporation and condensation,

$$r_v = \left(\frac{p_v\varphi}{RT_{sl}} - \frac{n_{wv} + \widehat{n}_{wv}}{2}\right)\frac{1}{\tau_v} \tag{6}$$

A positive value of r_v is defined to constitute evaporation; the symbol R is the ideal gas constant. It was found that calculating an arithmetic average of the non-smoothed and smoothed volumetric molar bulk density of vapor facilitates convergence. In addition, a soft constraint is imposed to limit the volumetric rate of evaporation to negative values (i.e. only allowing condensation) once the volumetric molar bulk density of liquid water approaches zero.

Table 1
Diffusivity of moisture in soil vs. moisture content.

Moisture [m^3/m^3]	Diffusivity [cm^2/day]
0	0.0
0.05	0.1
0.1	0.3
0.15	1.0
0.2	3.0
0.25	10
0.3	30

The heat of evaporation includes a correction for the difference between the solid/liquid temperature and gas/vapor temperature, and is defined as,

$$Q_v = r_v\left[M_w\left(\left(T_{sl} - T_{H_{v,0}}\right)\left(C_{p,wv} - C_{p,wl}\right) + H_{v,0}\right) + M_w C_{p,wv}(T_{av} - T_{sl})\right] \tag{7}$$

The relaxation in the temperature difference is imposed by defining a volumetric heat transfer relation between the respective domains of different phase,

$$Q_{\Delta T} = (T_{sl} - T_{av})\left(M_w C_{p,wv} n_{wv} + M_a C_{p,a} n_a\right)\frac{1}{\tau_v} \tag{8}$$

4.3. Model equations for transport phenomena

The transport of heat and moisture in soil is described by a set of five coupled diffusion equations. The default physics description of Comsol Multiphysics does not include the particular set of equations. Hence a custom set of model equations is implemented in this software package through its Partial Differential Equations (PDE) interface. The physics description is based on: the diffusion processes, flow through porous media according to Darcy's law (Eq. (9), and the ideal gas law (Eq. (10). To facilitate readability of the text, the complete derivation of the model equations is not presented in this section. This derivation is instead provided in Appendix B. This section continues by listing the model equations and the process variables that are associated with it.

The flow vector of gas and vapor in the soil volume is described by Darcy's law according to,

$$\overline{u}_{Darcy} = -\frac{k}{\mu\varphi}\nabla p \tag{9}$$

The ideal gas law includes φ to account for the porosity of soil; the symbol n generally represents the molar bulk density for an arbitrary gas or vapor,

$$p\varphi = nRT \tag{10}$$

Diffusion of liquid water governs the bulk molar density of liquid water n_{wl}. Its transport in soil is described by Eq. (11),

$$\partial_t n_{wl} + \nabla \bullet (-\alpha_w \nabla n_{wl}) + \overline{u}_0 \bullet \nabla n_{wl} + \frac{\alpha_w}{\alpha_s} n_{wl} = -r_v - r_{v,bc} + \frac{\alpha_w}{\alpha_s} n_{wl} \tag{11}$$

A new term $r_{v,bc}$ is introduced here. It represents the evaporation and condensation of moisture between ambient air and the topmost layer of soil. Section 4.4.4 discusses it in more detail in relation to the handling of boundary conditions in the simulation.

The temperature of soil and liquid water T_{sl} is governed by Eq. (12) according to,

$$\begin{aligned}&\partial_t T_{sl}\left(\rho_s C_{p,s} + M_w C_{p,wl} n_{wl}\right) + \nabla \bullet -\kappa\nabla T_{sl} + \left(\rho_s C_{p,s} + M_w C_{p,wl} n_{wl}\right)\overline{u}_0 \\ &\bullet \nabla T_{sl} + \frac{\kappa}{\alpha_s} T_{sl} \\ &= \frac{\kappa}{\alpha_s} T_{sl} - Q_v - Q_{v,bc} - Q_{\Delta T} + Q_{RF}\end{aligned} \tag{12}$$

This equation introduces a pair of new heat source/sink terms. In addition to variables Q_v and $Q_{\Delta T}$ (Section 4.2), the power density of radio wave heating Q_{RF} is introduced, as well as $Q_{v,bc}$, which is the latent heat of evaporation or condensation of moisture between ambient air and the topmost layer of soil. The term Q_{RF} is discussed in more detail in Section 5, while $Q_{v,bc}$ is discussed in relation to boundary equations modeling in Section 4.4.4.

The temperature of gas and vapor inside the soil volume – T_{av} – is

described by Eq. (13) according to,

$$\left(M_w C_{p,wv} n_{wv} + M_a C_{p,a} n_a\right)\partial_t T_{av} + \nabla \bullet -\kappa_{av}\nabla T_{av} + \left(M_w C_{p,wv} n_{wv} + M_a C_{p,a} n_a\right)\left(\frac{k}{\mu\varphi}\nabla p - \overline{u}_0\right) \bullet \nabla T_{av} + \frac{M_w C_{p,wv} n_{wv} + M_a C_{p,a} n_a}{\tau_v} T_{av} = \frac{M_w C_{p,wv} n_{wv} + M_a C_{p,a} n_a}{\tau_v} T_{sl} \tag{13}$$

Note that a new variable is introduced here. The term n_a represents the molar bulk density of air.

The pressure of gas and vapor inside the soil volume – p – is governed by Eq. (14),

$$\partial_t p + \nabla \bullet -\frac{k\widehat{p}}{\mu\varphi}\nabla p + \left(\frac{kp}{\mu\varphi}\frac{\nabla T_{sl}}{T_{sl}} + \overline{u}_0 - \frac{k}{\mu\varphi}\nabla\widehat{p}\right) \bullet \nabla p - \left(\frac{\nabla T_{sl}}{T_{sl}} \bullet \overline{u}_0 + \frac{\partial_t T_{sl}}{T_{sl}}\right) p = \frac{T_{sl} R}{\varphi} r_v \tag{14}$$

Finally, the bulk molar density of water vapor – n_{wv} – is described by Eq. (15),

$$\partial_t n_{wv} + \nabla \bullet -\alpha_v \nabla n_{wv} - \left(\frac{k\nabla p}{\mu\varphi} - \overline{u}_0\right) \bullet \nabla n_{wv} - \frac{k\nabla^2 p}{\mu\varphi} n_{wv} = r_v \tag{15}$$

4.4. Boundary conditions for transport phenomena

On the planes surrounding the soil volume, a set of boundary conditions are applied to account for the interactions of the transport processes with the surroundings. The planes in this discussion are defined according to Fig. 2.

Comsol Multiphysics allows for two types of boundary condition: a flux boundary condition, in which a gradient of a variable normal to the boundary is prescribed; and a Dirichlet boundary condition, in which a particular value for a variable is prescribed. With respect to a flux boundary condition, it can be defined as a gradient that is proportional to a variable, for example a heat transfer coefficient, or it can be defined as a gradient of fixed value. Regarding Dirichlet boundary conditions, these can also be left undefined so that no particular boundary condition is imposed.

Before boundary conditions can be defined, Section 4.4.1 analyses the diffusivities and characteristic lengths of the respective transport processes. This affects the selection of boundary condition types, as described in Sections 4.4.2–4.4.4 for the various planes that envelop the soil volume.

4.4.1. Diffusivity and characteristic length of transport processes

The selection of boundary condition for diffusion processes depends on the degree to which the effects of these processes reach the boundaries. If a particular process acts only locally and outside of the vicinity of a boundary, then the boundary condition for the associated variable may be fixed to an invariant value. Therefore, the diffusivity of the respective diffusion processes is first quantified, in order to assess the characteristic lengths of these processes. The thermal diffusivity of soil is at most $\kappa/(\rho C_p) = 0.44{\cdot}10^{-6}$ m^2/s (Mills, 1999); the diffusivity of liquid water in soil is at most $3.5{\cdot}10^{-8}$ m^2/s (Staple, 1965); the thermal diffusivity of air is $1.9{\cdot}10^{-6}$ m^2/s (Wikipedia, 2020) although this temperature is primarily coupled to the temperature of the solid/liquid domain; and the diffusivity of water vapor in air is $2.8{\cdot}10^{-5}$ m^2/s, (Wikipedia, 2019), although the molar bulk density of water vapor primarily depends on the local thermal equilibrium. Assuming a radio wave treatment process in the order of a minute, for these diffusivities the characteristic lengths would be respectively 5.1 mm, 1.4 mm, 10.7 mm, and 41 mm. These are all distances that will cause the effects of their associated processes to remain localized with respect to the soil volume. For pressure this is different though.

Combining the ideal gas law (Eq. (9), Darcy's law (Eq. (10) with the general mass balance for gasses and vapors,

$$\partial_t n = -n\nabla \bullet \overline{u}_{av} - \overline{u}_{av} \bullet \nabla n \tag{16}$$

yields,

$$\partial_t p = \frac{k}{\mu\varphi}\left(p\nabla^2 p + \nabla p \bullet \nabla p\right) \tag{17}$$

as a diffusion description for pressure. Assuming only small pressure variations close to pressure p_0 and linearization simplifies the expression to,

$$\partial_t p = \alpha_p \nabla^2 p \tag{18}$$

which corresponds to a plain linear diffusion equation with diffusivity,

$$\alpha_p = \frac{k p_0}{\mu\varphi} \tag{19}$$

For $k = 10^{-9}$ cm^2, $p_0 = 101325$ Pa, $\mu = 15$ μPa·s and $\varphi = 0.05$, the diffusivity is $\alpha_p = 1.35{\cdot}10^{-2}$ m^2/s. The characteristic length that is associated with this is 0.9 m. Consequently, pressure variations stretch over the width and depth of the simulated soil volume, and likely also beyond it.

4.4.2. Boundary conditions at the center, front, and back plane

Due to symmetry, a zero flux boundary condition can be applied to the center plane. The conditions at the front plane correspond to the initial conditions in soil, hence a Dirichlet boundary condition specifies for each variable its initial condition. At the back plane, unspecified Dirichlet boundary conditions are used, which is appropriate for the simulated situation in which conditions beyond the back plane cannot influence the soil volume, because of the imposed advection.

4.4.3. Boundary condition adjacent to soil

The bottom and side planes lie adjacent to soil beyond the simulated soil volume. An interaction with the soil outside of the simulated soil volume is feasible if the diffusion processes that are caused by radio wave heating can stretch to these planes. As per the discussion in Section 4.4.1, this can only occur for the gas and vapor pressure inside the soil volume. For the other variables, i.e. the solid/liquid temperature T_{sl}, the gas/vapor temperature T_{av}, the bulk molar density of liquid water n_{wl}, and of water vapor n_{wv}, the effects of the treatment process do not stretch to these planes. Hence, for those variables, Dirichlet boundary conditions are imposed that equal the initial conditions for each variable.

In contrast, for pressure a flux boundary condition is developed that approximates the response of soil beyond the simulated soil volume. This boundary condition is defined as,

$$-\overline{n} \bullet -\frac{\widehat{p}k}{\mu\varphi}\nabla p = -\sqrt{\frac{p_0 k \omega_{bc}}{2\mu\varphi}}(p - p_0) - \sqrt{\frac{p_0 k}{2\mu\varphi\omega_{bc}}} u_0 \partial_x p \tag{20}$$

In this equation, the symbol $\overline{n}$ represents the normal vector of the boundary plane; p_0 is the ambient pressure; ω_{bc} is the angular frequency characteristic for the treatment process. Preliminary simulation has estimated its value at 0.01 rad/s. Appendix C.1 presents the derivation of the expression for this boundary condition.

4.4.4. Boundary conditions at the top plane

A variety of descriptions is applied for the boundary conditions at the top plane that characterize the interactions between the soil volume and the ambient air. These are outlined as follows.

For the pressure of gas and vapor p, a Dirichlet boundary condition is applied that equals the pressure of ambient air.

The bulk molar density of water vapor n_{wv} is also defined at this boundary with a Dirichlet boundary condition, in this case as the corresponding value for vapor–liquid equilibrium with respect to the solid/

liquid temperature, i.e. $n_{wv} = \varphi f_A(T_{sl})/(RT_{sl})$.

For T_{av} an unspecified boundary condition is applied. This temperature does not significantly contribute to the overall balance of sensible heat due to the low thermal mass of gas and vapor with respect to the solid and liquid species in soil, therefore its effect on the overall heat balance is omitted.

The solid/liquid temperature, in contrast, does affect the heat balance significantly. A flux boundary condition is applied that describes natural convection of heat to the surroundings,

$$-\overline{n} \bullet (-\kappa \nabla T_{sl}) = -h_{n,T}(T - T_{amb}) \tag{21}$$

The calculation of the heat transfer coefficient for natural convection $h_{n,T}$ is provided in Appendix C.3. The convection coefficient is calculated to be 6.1 W/(m^{2}K).

For the bulk molar density of liquid water n_{wl}, a zero flux boundary condition is applied, as diffusion of liquid water will not occur into ambient air.

The evaporation and condensation of moisture to and from the ambient air also needs to be included in the simulation. The rate at which this occurs is defined by means of a convective mass transfer coefficient that is also calculated in Appendix C.3. Its value is determined to be $h_{n,m} = 6.36$ mm/s. Unfortunately, few options remain to represent this transfer of moisture with the standard boundary condition descriptions that are available in Comsol Multiphysics. Instead, an interaction layer is defined in the vicinity of the top plane for the transfer of moisture between the soil volume and the ambient air. In this interaction layer, the evaporation and condensation at the top plane is implemented as the volumetric source and sink terms $r_{v,bc}$ and $Q_{v,bc}$ that have already been introduced in Section 4.3. By employing the characteristic angular frequency of the treatment process ω_{bc} of 0.01 rad/s, a characteristic length for the influence of moisture transfer between the upper layers of the soil volume and the ambient air is calculated. The details of this calculation are presented in Appendix C.2; the resulting characteristic length is 9.4 mm. Accordingly, an interaction layer of 10 mm is imposed under the top plane where the surface flux of moisture due to evaporation and condensation is converted into the volumetric source/sink terms. Specifically, these terms $r_{v,bc}$ and $Q_{v,bc}$ are distributed in the interaction layer along a parabolic profile that falls to zero at the ultimate depth of this layer of 10 mm.

5. Electromagnetic model equations and implementation

The Radio-Frequency Module (RF-Module) of Comsol Multiphysics is used to simulate the radio wave field. This module solves the wave equation representation of Maxwell's electromagnetic field equations for the time harmonic electric field,

$$\nabla \times \left(\mu_r^{-1} \nabla \times \mathbf{E}\right) - k_0^2 \varepsilon_r \mathbf{E} = 0 \tag{22}$$

The electromagnetic field is represented by the electric field vector **E** in this equation. Analogous expressions that instead use the magnetic field vector **H** or the magnetic flux density vector **B** can be found in literature too. The symbol μ_r represents the relative magnetic permeability of the medium under consideration. In the context of this study no particular magnetic properties are considered, therefore $\mu_r = 1$, which is the relative permeability of vacuum. Soil, the medium under consideration, does have particular dielectric properties, so the relative dielectric permittivity ε_r determines propagation of radio wave energy and heat generation. In Eq. (22), k_0 is the free space wavenumber at the frequency of the field,

$$k_0 = \frac{\omega}{c_0} = \omega\sqrt{\varepsilon_0 \mu_0} \tag{23}$$

Here c_0 is the speed of light in vacuum, μ_0 the magnetic permeability of vacuum, ε_0 is the dielectric permittivity of vacuum. Medium properties are typically not expressed in absolute permittivity values, but in permittivity relative to vacuum. As such, the relative permittivity of vacuum is 1. The relative permittivity of a dissipative material like soil is a complex valued variable, i.e. $\varepsilon_r = \varepsilon' - i\varepsilon''$. Heat generation due to dissipation (Q_{RF}) depends on the loss factor ε'', angular frequency ω, and the intensity of the electric field vector **E** according to,

$$Q_{RF} = \frac{1}{2}\omega \varepsilon_0 \varepsilon'' \mathbf{E} \bullet \mathbf{E}^* \tag{24}$$

The next section describes the dielectric properties model that is applied in this study. For the interested reader, a more detailed discussion on the dielectric properties is included in Appendix D. Furthermore, the work by Pozar (2005) provides a good introductory text on electromagnetics and microwave engineering in case this is desired.

Fig. 4 presents the domain in which electromagnetic physics are simulated. The radio wave field is simulated in the antenna, in a soil domain under the antenna, and in an air domain around the antenna. The simulation domain is enclosed in a perfectly matched layer that simulates the wider surroundings by absorbing the field as it travels beyond the direct vicinity of the antenna.

6. Dielectric medium model

Section 5 describes the model equations that are used to simulate the radio wave field. It also introduces the dielectric properties, and shows how they appear in these equations. In all, the narrative of Section 5 is straightforward, because it is a brief outline of the default implementation of the RF–Module of Comsol Multiphysics. The discussion on the dielectric medium model is more involved, though. There are no model databases available for dielectric properties of horticulture soils at 915 MHz. In lieu of pre-existing data, and in accordance with the framework approach of this study, a model is developed that provides an adequate initial description of the dielectric properties. Subsequently, in later works, this initial description can be iterated upon to provide a more accurate description of the medium properties in specific horticulture soils. This section proceeds by first outlining the medium properties measurement of soil via the coaxial probe method, and by then describing how dielectric models are fitted to this measurement data. In summary, a dielectric mixing model is developed that allows for the evaluation of variation of 1) temperature; 2) moisture content; 3) salinity; and 4) porous volume.

6.1. Properties measurement of compressed soil

The dielectric properties of three soil samples are measured. These are glasshouse horticulture samples, two samples at different humidity have been obtained from a glasshouse horticulture company, a third is prepared by drying a portion of one of the original samples. The dielectric properties are measured over a 500 MHz to 5 GHz interval. The measurement equipment is an Agilent 85070E kit with performance probe option connected to an Agilent E5071C network analyzer and an

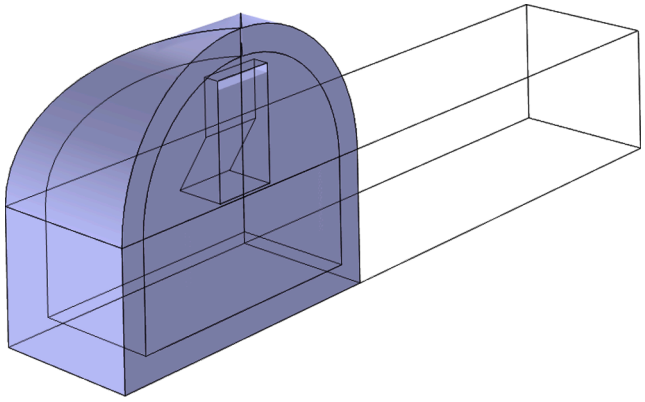

Fig. 4. Spatial domain of electromagnetic field simulation (dark color).

Agilent N4691B ECal module. The probe is pressed into the soil sample with consistent force so that sufficient contact is achieved. Fig. 5 presents the spectral measurements of the three soil samples.

A parametrized dielectric model is fitted onto the measured spectra in Fig. 5. This model is the single relaxation Debye dielectric model with a conductivity term added to it (Kremer & Schönhals, 2003). This was found to provide a suitable fit in the 500–2000 MHz frequency range. This single relaxation model with conductivity term is expressed as,

$$\varepsilon(\omega) = \varepsilon_\infty + \frac{\varepsilon_s - \varepsilon_\infty}{1 + i\omega\tau} - i\frac{\sigma}{\varepsilon_0\omega} \tag{25}$$

where ε_∞ is the real part of the permittivity approximated at infinite frequency, ε_s is the static permittivity, τ is the time constant of the dielectric relaxation, and σ is the electrical conductivity. The undulations that are present in the dielectric spectra are measurement artifacts that are not representable in the model equation. Hence, the parametrized fit filters out these undulations, and allows for a more precise determination of the medium properties at a specific frequency. Table 2 lists the model parameters and filtered relative permittivity for the three soil samples at 915 MHz. On a side note, the conductivity term is appreciable, which suggests that conductivity losses caused by salts dissolved in the water content of the soil contribute a significant portion of the overall heat generation.

6.2. Effective medium model for heterogeneous soil

Two dielectric mixing models are commonly used to determine the dielectric properties of heterogeneously mixed media. These models are the Maxwell-Garnett formula and the Bruggeman formula presented in Eqs. (26) resp. 27 below (Sihvola, 1999).

$$\varepsilon_{eff} = \varepsilon_e + 3f\varepsilon_e\frac{\varepsilon_i - \varepsilon_e}{\varepsilon_i + 2\varepsilon_e - f(\varepsilon_i - \varepsilon_e)} \tag{26}$$

$$\sum_{j=1}^{N} f_j\frac{\varepsilon_j - \varepsilon_{eff}}{\varepsilon_j + 2\varepsilon_{eff}} = 0 \tag{27}$$

Both these equations assume the heterogeneous mixture to consist of spherical inclusions of a particular dielectric medium inside an environment of a different dielectric medium. The two approaches are different though. The Maxwell-Garnett approach applies only to binary mixtures, in which one species of this mixture forms the inclusion, and the other the environment. The Bruggeman approach is to consider all species inclusions, with the environment having dielectric medium

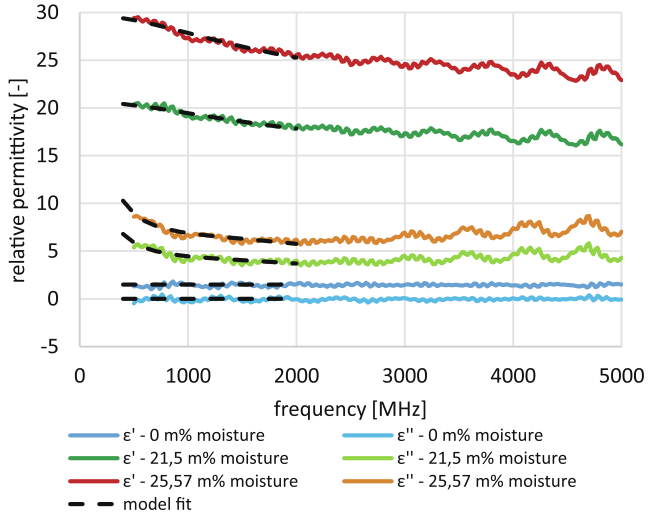

Fig. 5. Dielectric spectra of soil samples at 0 m%, 21.50 m%, and 25.57 m%. The spectra are measured with Agilent equipment: an 85070E performance probe kit, an E5071C network analyzer, and an N4691B ECal module.

Table 2
Dielectric model fit, measurements were performed at 20 °C.

sample	0 m%	21.50 m%	25.57 m%
ε_s [-]	1.5	11.95	17.21
ε_∞ [-]	1.5	8.86	12.05
τ [ps]	0	95.92	105.42
σ [mS/m]	0	80.35	115.62
ε at 915 MHz [-]	1.5 – 0i	19.6 – 4.57i	28.10 – 7.04i

properties equal to the mixed dielectric properties. The Bruggeman approach allows for an indefinite number of species. However, it is an implicit formula, which is less conveniently implemented than the Maxwell-Garnett formula. Sihvola (1999) presents a study that compares several dielectric mixing formulas to a finite difference time domain FDTD simulation of a heterogeneous mixture, and shows that the Bruggeman approach performs best. In the Maxwell-Garnet formula, ε_{eff} are the effective or mixed dielectric properties, ε_e are the dielectric properties of the environment species, ε_i are the properties of the inclusion species, and f is the volume fraction of the inclusions. In the Bruggeman formula, ε_{eff} are the effective or mixed dielectric properties, ε_j are the properties of the j-th species, and f_j is the volume fraction of the j-th species.

With these formulas, the properties of the individual species in the measured samples are estimated. The conductivity contributions are subtracted; and using the inverted Bruggeman formula and dielectric reference data for water from Kaatze (1989) and the known water content of the samples, the contributions for dry soil are calculated. In doing so, it turned out that the contributions of dry soil did not converge towards a constant value. It was therefore concluded that the assumptions behind the dielectric mixing models do not strictly hold. This could be caused by a non-spherical morphology of the species, or by chemical and/or physical bonding between species. Detailed investigation of the relations between moisture content and dielectric properties of soil would lead out of the scope of the present study. Instead an expedient approach is taken by making the dielectric contribution of soil dependent on moisture content. A single relaxation Debye parametrization with conductivity term is fitted to the dielectric contributions of dry soil, and a function (f_c) is defined based on a simple exponential curve (Eq. (28) to interpolate the parametrizations between moisture levels. The function varies with the ratio of moisture to total weight $\frac{m_w}{m_t}$ expressed in mass percentage. Table 3 presents the function coefficients C_5 to C_7 for the respective Debye parameters.

$$f_c\left(\frac{m_w}{m_t}\right) = C_5 + C_6 e^{\frac{m_w}{m_t}C_7} \tag{28}$$

With the data obtained so far, the respective contributions of the heterogeneous soil mixture can be combined to calculate to the effective dielectric medium properties: Equation (28) provides the parameters for a single relaxation Debye model with conductivity term. These parameters are then applied to Equation (25) to calculate the properties of dry soil. The temperature dependent dielectric properties of water at 915 MHz are calculated from reference data from Kaatze (1989). For the properties of the porous volume of soil that contains air, vapor and/or gasses the permittivity of vacuum is a suitable approximation.

In the overall simulation, the Bruggeman formula is not practical because it is an implicit relation, despite the fact that it is reported to give a more accurate estimation that the Maxwell-Garnett approach. It is

Table 3
Dry soil model parameters.

	C_5	C_6	C_7
ε_s [-]	– 0.384	1.883	0.0874
ε_∞ [-]	– 0.483	1.983	0.0721
τ [ps]	149.98	– 149.98	– 0.0475
σ [mS/m]	– 20.86	20.86	0.0734

instead used as a reference to determine the best manner in which the Maxwell-Garnett formula can be applied.

The effective permittivity of the heterogeneous mixture is determined by first calculating the permittivity of the non-porous soil and water mixture. It was found that for the real relative permittivity of the soil/water mixture, the Maxwell-Garnett formula with water as inclusion works best. For the imaginary part of the relative permittivity the best correspondence was found by calculating the permittivity twice, once with water as inclusion, and once with soil as inclusion, and by calculating the average of the resulting two imaginary numbers.

The contribution to electromagnetic dissipation and heat generation due to conduction is subsequently added to the loss factor (the imaginary part of the soil/water effective dielectric permittivity). The exact ionic content is not known, therefore an equivalent NaCl contribution is calculated. It is found that the conductivity term of the 21.50 m% sample corresponds to an equivalent of a 0.058 %ds of NaCl. The equivalent NaCl concentration is determined at 13.34 mM by correlating the conductivity value of 80.35 mS/m to data from Polle and Chen (2015). The salinity contribution to the loss factor is determined by linearly scaling from these values.

Finally, the effect of the porous volume of air and vapor in the soil was implemented via the Maxwell-Garnett formula with air as inclusion in a non-porous mixture of soil and saline water.

7. Pathogen inactivation model

An Arrhenius expression is employed for the thermal inactivation model for pathogens in this study. There are valid criticisms for this choice, but there is also an advantage to it. As for the criticism, in their review, Peleg et al. (2012) correctly point out that it was "originally derived for reactions between gas molecules or molecules in solution [and] should not be used in lieu of its independent validation". Moreover, the authors correctly identify the "conceptual problems and practical deficiencies" of the Arrhenius model, in particular the incongruity of specifying an activation energy "per mole" of biological life, and the use of the ideal gas constant despite the fact that biological entities are many orders of magnitude heavier than gas molecules and equally more complex.

Nevertheless, the Arrhenius expression is a familiar concept in the fields of energy production and engineering of energy systems. This facilitates a common language between these fields and the biological disciplines, in which these expressions are nevertheless adopted for the prediction of organism inactivation, despite the fact that alternative models are available (Peleg, et al., 2012) (Fujikawa & Itoh, 1998) (Pullman, et al., 1981). We are of the opinion that a common language is a notable advantage, and hence the Arrhenius model is adopted in our present study too.

Fujikawa and Itoh (1998) report on pathogen inactivation described via a first order Arrhenius expression. They demonstrate the adequacy of the approach by fitting such an expression on data reported by Pullman et al. (1981) on four fungal pathogens: *R. solani*, *V. dahliae*, *P. ultimum* and *T. basicola*. The model expression is found to be consistent with the data for the respective pathogens.

It is this model fit that is used as the Arrhenius expression for pathogen inactivation in this present study. The temperature dependence of the inactivation rate constant is,

$$k(T) = k_{T_{ref}} \exp\left[\frac{E_a}{R}\left(\frac{1}{T_{ref}} - \frac{1}{T}\right)\right] \tag{29}$$

here $k_{T_{ref}}$ is the rate constant at a specified reference temperature T_{ref}. This resulting temperature dependent rate constant $k(T)$ expresses the exponential decay in pathogen population N,

$$N(t) = N_0 e^{-k(T)t} \tag{30}$$

which corresponds to the following first order differential equation,

$$\partial_t N = -k(T)N \tag{31}$$

which suggests an exponentially decaying relation. Exponential variations that change over many orders of magnitude are more conveniently expressed on a logarithmic base in order to maintain the feasibility of their numerical representation. Therefore the following transformation is applied,

$$\log_{10} N = N_L\,,\ N = 10^{N_L} \tag{32}$$

Substitution and rearranging yields,

$$\partial_t(N_L) = -\frac{k_{T_{ref}} \exp\left(\frac{E_a}{RT_{ref}}\right)}{\ln 10} \exp\left(-\frac{E_a}{RT}\right) \tag{33}$$

At the starting point of the treatment, the population has experienced no inactivation. The pathogen number is expressed relative to its initial number, i.e. $N_0 = 1$, and $N_{L,t=0} = 0$. Integration over time yields,

$$N_L(t) = -\frac{k_{T_{ref}} \exp\left(\frac{E_a}{RT_{ref}}\right)}{\ln 10} \int_0^t \exp\left(-\frac{E_a}{RT(t)}\right) dt \tag{34}$$

The model parameters are derived from Pullman et al. (1981) and are applied in this present study as follows: $E_a = 5.333{\cdot}10^5$ J/mol, $k_{T_{ref}} = 11.51$ 1/h, $T_{ref} = 48.52$ °C. The temperature profiles simulated in Comsol Multiphysics are exported into the Matlab environment to evaluate the integral expression in Eq. (34).

Fig. 6 shows curves of pathogen inactivation versus temperature at four different durations of exposure. These curves are calculated with Eq. (34); The durations of exposure vary from 10 s to 2 h. The threshold temperature at which the pathogens are inactivated depend on the duration of exposure. Since radio wave treatment is a more rapid process than steam treatment, it can be expected that due to the reduced process time, the threshold temperature will be higher.

8. Process simulation and evaluation of modeling approach

The simulation approach described in the previous sections is demonstrated by simulating a treatment process with the antenna moving at 6 mm/s over the soil, a power output of 56 kW over the width of the antenna, and a soil humidity of 21.5 m%. Note that the power level of 56 kW was imposed on the entire antenna, not just the simulated symmetrical half; consequently, the simulated antenna half had 28 kW imposed on its input port. Soil porosity is 5 %, and the free ion content is 0.058 %ds NaCl equivalent, i.e. mass percent of dry soil. The initial soil temperature is 10 °C, and the temperature of ambient air is 20 °C at a relative humidity of 40 %.

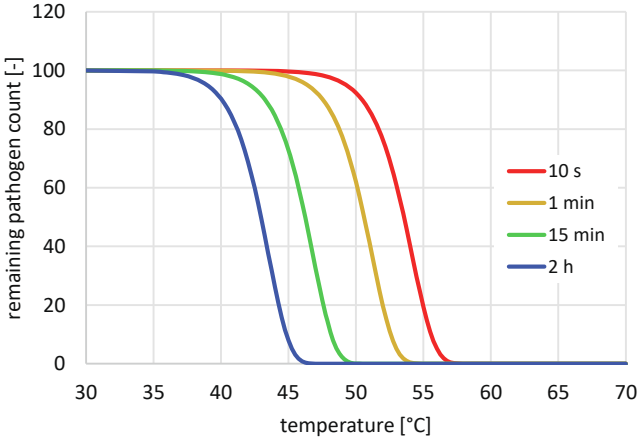

Fig. 6. Model calculation of pathogen inactivation versus temperature at various durations of exposure.

This section proceeds with discussions on: the simulation results and the resulting simulated treatment depths; the performance of the simulated antenna versus the antenna design that is used in the Agritron prototype (Fig. 1); and an evaluation of simulated transient.

8.1. Simulation results and treatment depth

The simulation results show how the radio wave field is transmitted from the antenna into the soil, how the radio wave energy decays as it travels into the soil, and how it is partially scattered towards the surroundings (Fig. 7a). The decay of radio wave energy causes heat generation inside the soil underneath the antenna (Fig. 7b), and the formation of a track of elevated temperature behind the antenna (Fig. 8a). Evaporation of moisture forms an area of elevated pressure in front of the antenna, while a zone of reduced pressure forms behind the antenna (Fig. 8b). The effect on the moisture balance of the treatment process shows a quick response in the bulk density of water vapor (Fig. 9a), while a delayed effect occurs for liquid moisture (Fig. 9b). The bulk molar density of water vapor is proportional to the vapor pressure, which is directly related to temperature. Hence, water vapor density forms a similar track of elevated values as temperature does. In contrast, the liquid fraction of moisture in soil is only gradually reduced by evaporation in a shallow top layer of soil above the track of elevated temperature. This may allow for a simplification in the manner in which the dielectric permittivity of soil is modeled. In the zone directly underneath the antenna, there is little alteration in the fraction of liquid moisture. Therefore, dynamic variation of the dielectric properties due to alteration of the moisture fraction may possibly be omitted from the simulation.

Pathogen inactivation contours show a treatment effect that progresses rapidly during the first minutes of the treatment (Fig. 10). It reaches a depth of 4 to 5 cm into the soil for the particular set or treatment parameters that was simulated. In the hours following radio wave exposure, only little additional treatment effect is gained, which demonstrates the swift dynamic nature of radio wave treatment. The associated threshold temperature that corresponds to the depth of treatment is approximately 60 °C.

In order to verify whether the simulation approach can replicate treatment depths that have been observed during field trials, a second simulation has been performed that applies more radio wave energy. Specifically, the treatment parameters are: a vehicle velocity of 0.2 m/min or 3.33 mm/s; a radio wave power of 100 kW; a soil humidity of 10 m%, and a salinity of 0.058 %ds NaCl equivalent. In addition, a pretreatment of the soil was applied that exposes the soil for 72 h to ambient air of 20 °C and 40 % relative humidity. Consequently, the starting temperature of soil is higher and the threshold is reached more easily. Furthermore, the moisture content of the top soil layer is lower, so that less radio wave energy is dissipated in this layer and more of it is allowed to travel deeper into the soil. With these parameters, a deeper treatment is achieved (Fig. 11). Two minutes after the initial exposure the treatment depth is approximately 12 cm. In the hours after exposure, the heat that was introduced travels deeper into the soil and extends the treatment depth to about 15 cm. These depths are in line with pathogen effects that have been observed during field trials (Staalduinen, 2022). In accordance with the first simulation, the majority of the treatment effect is achieved during the first minutes.

8.2. Antenna efficiency, simulated geometry versus prototype

With respect to the efficiency of this particular antenna configuration and its simulated performance, some clarifications need to be included here. A standing wave pattern is apparent in the horn antenna (Fig. 7a), which is indicative of a reflection loss, i.e. an amount of radio wave energy scattered back towards the radio wave source after reflection upon the soil surface. In addition, the emission of radio wave energy towards the surroundings above soil constitute an emission loss. The reflection and emission losses of the simulation amount to 35.7 % and 3.64 % respectively. These figures relate to the simplified antenna geometry that is used to develop the simulation approach. *These numbers, however, bear no relevance with respect to the performance of the prototype depicted in* Fig. 1*; the prototype design has features similar to the simulated antenna geometry, but it is distinctly different and includes additional design features that counteract the aforementioned losses.* The antenna geometry that is used in the simulation is chosen because it presents a relevant antenna design, while avoiding the need to disclose proprietary design features of the prototype. Furthermore, it enables the use of software packages that are under academic license, because it avoids simulation of a commercial prototype. *To avoid any confusion, by no means do we want to suggest that the efficiencies of the simulated antenna are indicative in general for any radio wave heating systems of soil. The particular antenna design in the simulation was chosen for expediency, not for a high efficiency.* To further elaborate the point, the Agritron prototype has demonstrated in field studies the ability to be tuned to reduce the reflection loss to close to zero. Moreover, during field studies, radio wave field emissions have been verified to fall well below action levels of maximum allowable radio wave emission. Specifically, at the operating frequency of 915 MHz the action level for the radio wave energy flux is 22.9 W/m^2 (European Parliament and Council, 2013). Measurements around the prototype confirm that this value is not reached. These are performed both with a ETS-Lindgren HI-1600 survey meter as well as a Siglent

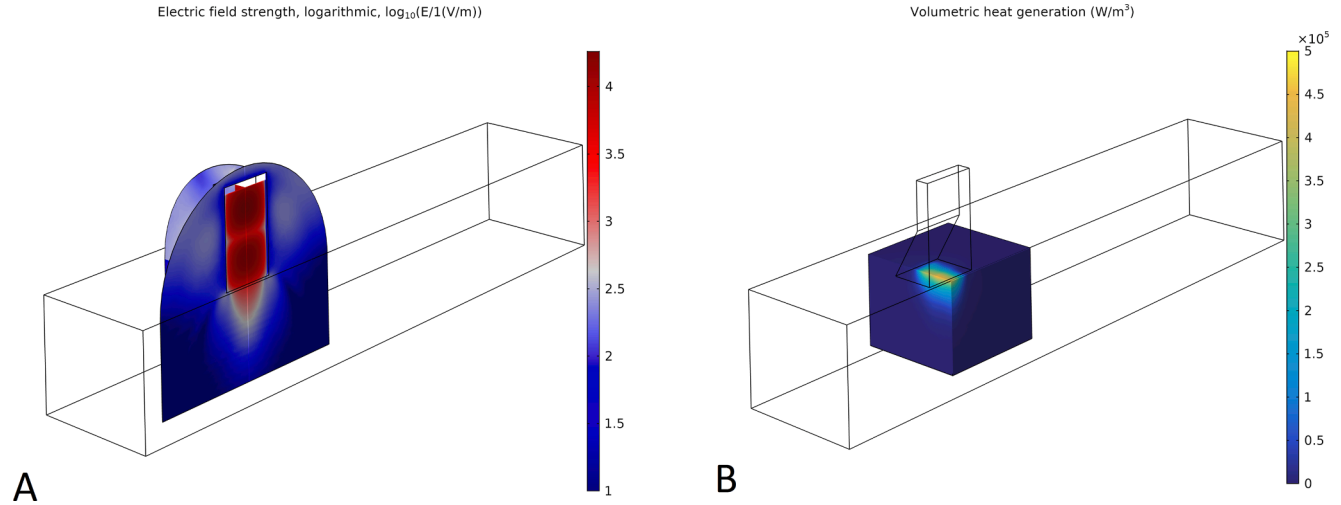

Fig. 7. Simulated electromagnetic effects, left (a): logarithm of the electric field amplitude; right (b): volumetric heat generation due to radio wave heating.

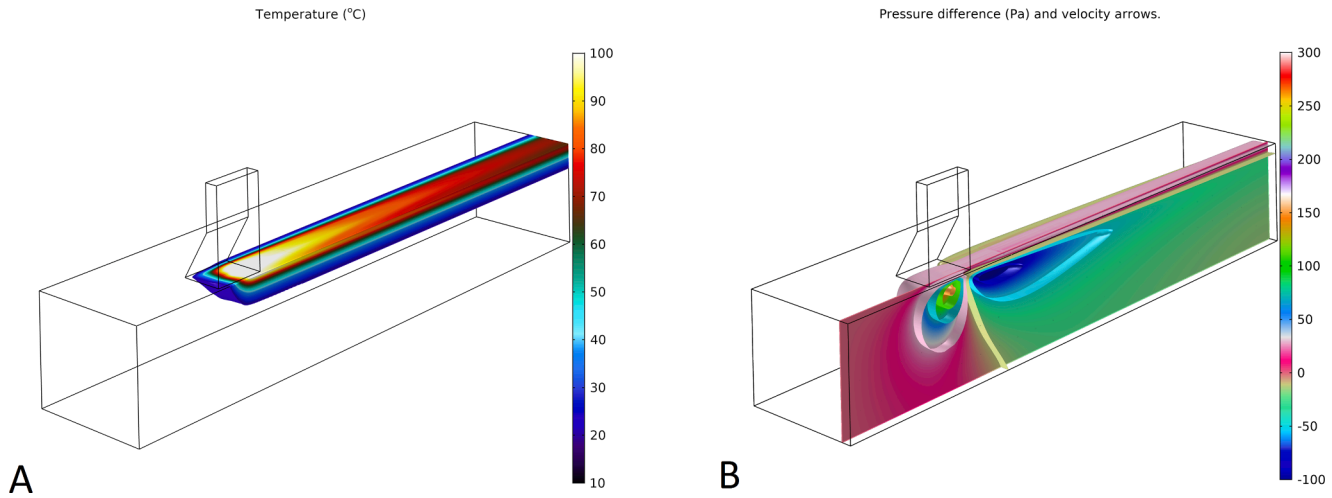

Fig. 8. Simulated temperature (left, a) and pressure (gauge, right, b) is the soil volume that is being treated with radio wave energy.

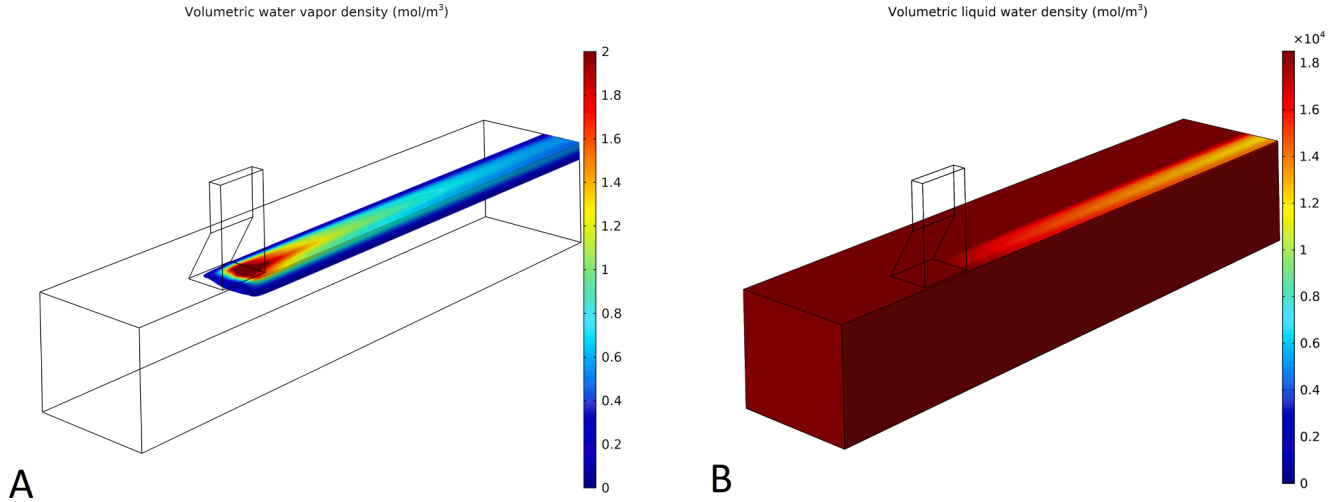

Fig. 9. Moisture bulk density variations, left: water vapor; right: liquid water.

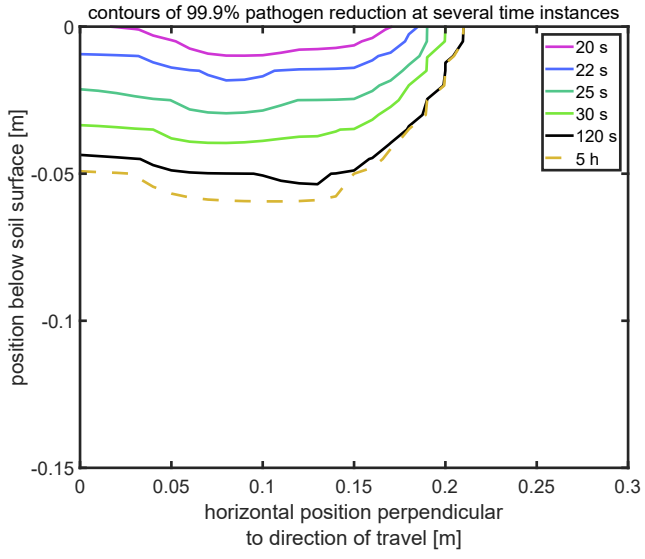

Fig. 10. Simulated pathogen inactivation in a soil cross section at various time instances after the start of treatment.

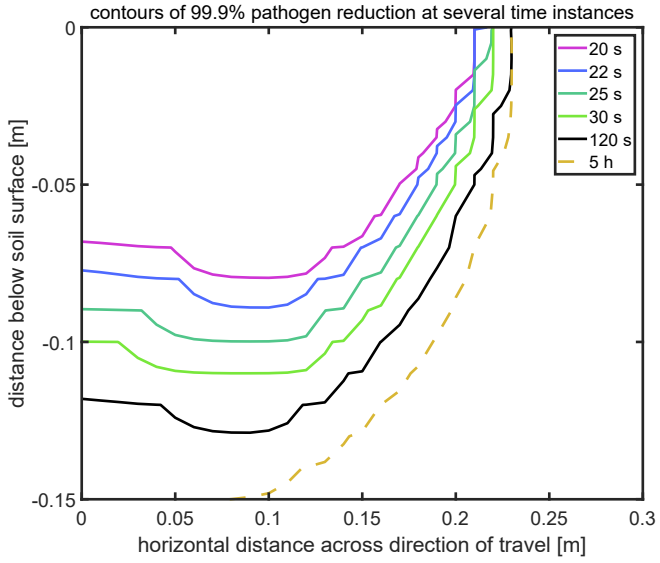

Fig. 11. Simulated pathogen inactivation for the second simulation that applies more energy. The contours are drawn over a soil cross section at various time instances after the start of treatment.

SVA1015X spectrum and vector network analyzer in combination with a Texbox TBPS01 probe kit.

8.3. Transient evaluation

Simulated temperature and pressure transients from the first simulation are juxtaposed to transients measured during two separate field trials at different horticulture companies. One of the trials recorded temperature, the other pressure. The temperature recordings were performed with a set of three Rugged Monitoring Lsens-U fiber optic temperature sensors positioned vertically aligned at depths of 20 mm, 40 mm, and 100 mm under the path of the Agritron prototype. Pressure was measured with a SMC PSE543A pressure transducer connected to a length of pneumatic tube of 6 mm outer diameter. The open end of the tube was placed at a depth of around 10 cm in the soil under the path of the Agritron prototype; the end with the pressure transducer was kept outside the path of the Agritron vehicle to avoid interference of the radio wave field on the pressure transducer.

There is similarity between the experimental and simulated temperature transients, but they are not exactly the same. The measured temperature transients have different dynamics following the application of radio wave energy compared to the simulated ones (Fig. 12). Moreover, the experimental transients have greater temperature development at the deeper 100 mm depth. The pressure transients also differ considerably. Soil of the field trial has a much higher pressure increase and the pressure recording has strong fluctuations (Fig. 13). These differences are likely due to a mismatch in Darcy permeability, but also due to soil deformation that occurred during the field trial as the prototype vehicle travels over it.

A final aspect on model validity that is evaluated here is the coupling between the solid/liquid and gas/vapor phase domains. These simulated temperature and pressure transients are overlaid in Fig. 14. The temperature transients have similar shape, but have an approximately constant gap between them. This temperature difference maintains the heat transfer between the two domains of different phase. A smaller time constant for coupling between the domains (τ_v, Eq. (4), 6, and 8) would have reduced the difference, though this would require a finer spatial discretization of the soil domain in order to maintain numerical stability. The temperature difference would not be detrimental to the overall energy balance however. Moreover, unlike the temperature curves, the transients for equilibrium vapor pressure and actual vapor pressure show closer agreement.

In summary, for as far as can be evaluated at this point, the simulation approach provides an adequate representation of the radio wave treatment process. Differences with respect to experimental data can tentatively be attributed to a mismatch with the physical and biological parameters. This would advocate for the development of instruments to quantity these parameters. The spatial resolution of the simulation is restricted by the computational constraints that are imposed on it. If it would be required for a particular study, a better resolution can surely be achieved, provided that the increased computational expense is supported. In case the motion of the antenna with respect to soil is no longer accounted for by soil advection, but instead by the deformable mesh feature of Comsol Multiphysics and if a much finer mesh is applied, then stabilization by smoothing could likely be omitted. This would however also increase computational expense. In addition, to achieve a particularly high resolution, a small volume section of soil could be represented by a heterogeneous porous geometry to better approximate soil physics. Likewise a more involved model could be developed for the release of nutrients and for biological effect. Such refinements could be subject of follow-up studies. In any case, the present model enables an extensive parametric study to evaluate the effect of physical process variations, which will be subject of a next work.

9. Conclusions

A model is developed that simulates heating and transport phenomena in soil during radio wave treatment of soil. This model is a simulation framework that combines relevant physical and biological processes. It is a starting point for model refinement that can be adapted to specific treatment cases, although in its present form it does not match a specific case. The model is intended to aid in the development of radio wave treatment for pathogen suppression in glasshouse horticulture. It facilitates development of all design aspects of the treatment process, comprising of the radio wave equipment, the integration with renewable energy sources, development of treatment strategies for specific horticulture cases, and adaptation of the soil structure to optimize the effectiveness of the application of radio wave energy. The modeling framework is Comsol Multiphysics in combination with Matlab, and the computational requirements are limited to workstation grade hardware. Simulation results are presented to demonstrate the simulation. The modeling framework enables a parametric study to gain insight into how the respective process parameters affect the treatment process, and into what prioritization the parameters need in relation to the development of the overall treatment process, which will be the topic of a subsequent study.

Author contributions

The research was performed as part of a collaborative project

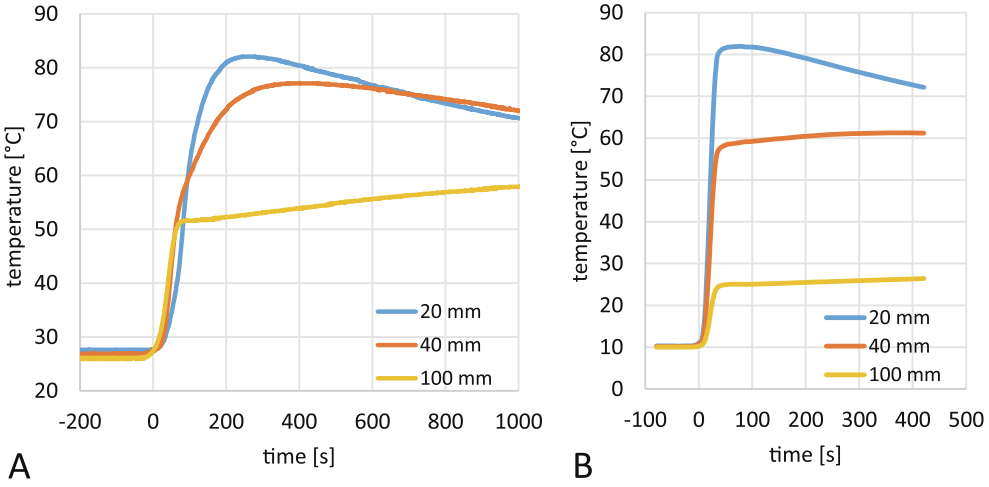

Fig. 12. Measurement of temperature in soil during a field trial (a), and simulated temperature transents at the same depths (b). A set of Rugged Monitoring Lsens-U fiber optic temperature sensors was used to record the temperarures.

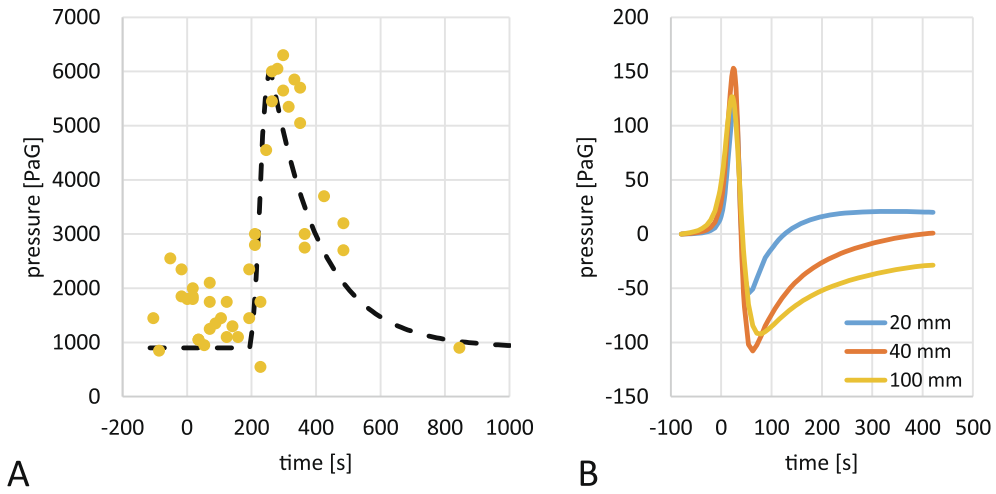

Fig. 13. Measurements of pressure at a depth of 10 cm during a field trial (left), and simulated pressure transients (right). A SMC PSE543A pressure transducer was used for the measurement. The dashed line is included to guide the eye.

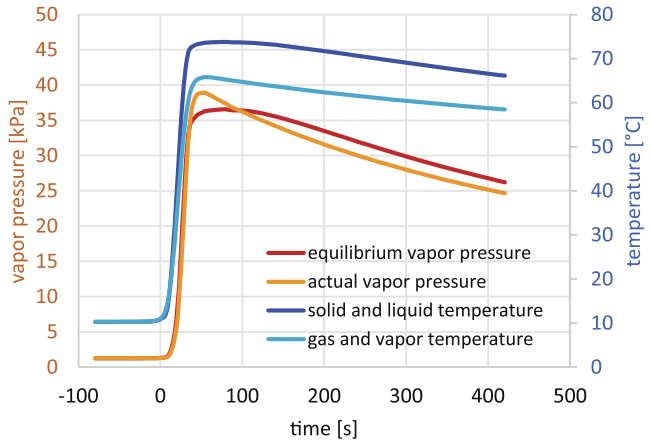

Fig. 14. Comparison of simulated transients for temperature and vapor pressure between the gas/vapor and solid/liquid domains.

between Koppert Machines (KM), Stichting Control in Food & Flowers (SCFF), Groen Agro Control (GAC), and Delft University of Technology (DUT). The roles in relation to this present study are: G. Sturm (DUT), numerical model development, writing; J. Bonnet (SCFF) and A. v.d. Wurff (GAC), biological tests; A. Koppert and S. Linnenbank (KM), preparation and operation of prototype in field trials.

Declaration of Competing Interest

The authors declare that they have no known competing financial interests or personal relationships that could have appeared to influence the work reported in this paper.

Data availability

Data will be made available on request.

Acknowledgments

This research was performed in the framework of Kas als Energiebron, the Dutch innovation and action programme for saving energy and applying sustainable energy in greenhouse horticulture of Glastuinbouw Nederland and the Dutch Ministry of Agriculture, Nature and Food Quality. Contract number 1400 0103 54, reference number DGA-PAV / 1917 8589.

Our thanks go out to Tuinbouwbedrijf A. Baatje b.v. and MC GRAND b.v. for facilitating field trials, and for providing soil samples.

Our thanks also go out to Prof. Rene Pecnik of the Process & Energy department of Delft University of Technology for feedback on the model description for transport phenomena, and to Bart Hoek, same department, for continued support.

Appendix B. Derivation of transport equations.

The transport phenomena in soil are presented by a custom set of partial differential equations that are expressed via the PDE interface of the mathematics module of COMSOL Multiphysics. The coefficient form PDE option is used, which requires the system equations to be expressed as second order differential equations of the general form,

$$d_a\partial_t\mathbf{u}+\nabla\bullet(-c\nabla\mathbf{u})+\beta\bullet\nabla\mathbf{u}+a\mathbf{u}=f \tag{35}$$

The subsequent sections of this appendix details the derivation of the custom differential equations for transport equations.

B.1. Mass balance of liquid water

For liquid water diffusion, convection due to the advection of soil under the antenna, and the volumetric evaporation of water are combined into the following equation,

$$\partial_t n_{wl}=\alpha_w\nabla^2 n_{wl}-\overline{u}_0\bullet\nabla n_{wl}-r_v-r_{v,bc} \tag{36}$$

The term $r_{v,bc}$ accounts for the evaporation to and condensation from the ambient air above the soil. The manner in which these boundary

conditions are imposed are discussed in Section 4.4.4. The equation is brought into a form suitable for the coefficient form PDE interface in accordance with Eq. (35),

$$\partial_t n_{wl} + \nabla \bullet (-\alpha_w \nabla n_{wl}) + \overline{u}_0 \bullet \nabla n_{wl} = -r_v - r_{v,bc} \tag{37}$$

and additional terms to the left and right of the equation are added to improve stability,

$$\partial_t n_{wl} + \nabla \bullet (-\alpha_w \nabla n_{wl}) + \overline{u}_0 \bullet \nabla n_{wl} + \frac{\alpha_w}{\alpha_s} n_{wl} = -r_v - r_{v,bc} + \frac{\alpha_w}{\alpha_s} n_{wl} \tag{38}$$

B.2. Heat balance in soil and liquid water

For mathematical simplicity in this study the enthalpy is defined with reference to 0 K. The expression for sensible enthalpy of the solid/liquid domain is the sum of the sensible enthalpy of soil and liquid water,

$$H_{s,sl} = T_{sl}\left(\rho_s C_{p,s} + M_w C_{p,wl} n_{wl}\right) \tag{39}$$

Several factors affect this variable over time. These are expressed as time derivatives of the constituent parts of this enthalpy and volumetric heat source or sink terms. The terms make up the overall enthalpy balance according to the following equation,

$$\partial_t H_{s,sl} = \partial_t H_{s,sl,dc} + \partial_t H_{s,sl,cc} + \partial_t H_{s,sl,hc} - Q_v - Q_{v,bc} - Q_{\Delta T} + Q_{RF} \tag{40}$$

The terms Q_v and $Q_{\Delta T}$ are volumetric heat source and sink terms for the heat of evaporation and heat transfer between the solid/liquid domain and gas/vapor domain. These are described in Section 4.2. The term $Q_{v,bc}$ represents the latent heat of evaporation and condensation between the soil surface and the air above it; this term is discussed in Section 4.4.4. The final source term – Q_{RF} – is the heat generation by the radio wave field, which is discussed in Section 5 (Eq. (24).

The term $\partial_t H_{s,sl,dc}$ expresses the transport of heat along with the transport of liquid water due to diffusion, moisture gradient advection with the soil, and evaporation,

$$\partial_t H_{s,sl,dc} = T_{sl} M_w C_{p,wl}\left(\alpha_w \nabla^2 n_{wl} - \overline{u}_0 \bullet \nabla n_{wl} - r_v\right) \tag{41}$$

The term $\partial_t H_{s,sl,cc}$ expresses heat transport due to temperature gradients advection with soil,

$$\partial_t H_{s,sl,cc} = -\left(\rho_s C_{p,s} + M_w C_{p,wl} n_{wl}\right) \nabla T_{sl} \bullet \overline{u}_0 \tag{42}$$

The term $\partial_t H_{s,sl,hc}$ expresses the conduction of heat in soil,

$$\partial_t H_{s,sl,hc} = \kappa \nabla^2 T_{sl} \tag{43}$$

The model equation is derived as follows. Differentiation of Eq. (39) to time yields,

$$\partial_t H_{s,sl} = \partial_t T_{sl}\left(\rho_s C_{p,s} + M_w C_{p,wl} n_{wl}\right) + T_{sl} M_w C_{p,wl} \partial_t n_{wl} \tag{44}$$

Eq. (37) is substituted into Eq. (44),

$$\partial_t H_{s,sl} = \partial_t T_{sl}\left(\rho_s C_{p,s} + M_w C_{p,wl} n_{wl}\right) + T_{sl} M_w C_{p,wl}\left(\alpha_w \nabla^2 n_{wl} - \overline{u}_0 \bullet \nabla n_{wl} - r_v\right) \tag{45}$$

Further substitution of Eqs. (40)–(43) into Eq. (45) is applied,

$$\partial_t T_{sl}\left(\rho_s C_{p,s} + M_w C_{p,wl} n_{wl}\right) + T_{sl} M_w C_{p,wl}\left(\alpha_w \nabla^2 n_{wl} - \overline{u}_0 \bullet \nabla n_{wl} - r_v\right) = T_{sl} M_w C_{p,wl}\left(\alpha_w \nabla^2 n_{wl} - \overline{u}_0 \bullet \nabla n_{wl} - r_v\right) - \left(\rho_s C_{p,s} + M_w C_{p,wl} n_{wl}\right) \nabla T_{sl} \bullet \overline{u}_0 + \kappa \nabla^2 T_{sl} - Q_v - Q_{v,bc} - Q_{\Delta T} + Q_{RF} \tag{46}$$

Rearranging the equation and eliminating terms yields,

$$\partial_t T_{sl}\left(\rho_s C_{p,s} + M_w C_{p,wl} n_{wl}\right) = -\left(\rho_s C_{p,s} + M_w C_{p,wl} n_{wl}\right) \nabla T_{sl} \bullet \overline{u}_0 + \kappa \nabla^2 T_{sl} - Q_v - Q_{v,bc} - Q_{\Delta T} + Q_{RF} \tag{47}$$

Additional rearrangement is applied to bring the equation into a form suitable for the PDE interface. In addition terms are added left and right of the equation to improve stability,

$$\partial_t T_{sl}\left(\rho_s C_{p,s} + M_w C_{p,wl} n_{wl}\right) + \nabla \bullet -\kappa \nabla T_{sl} + \left(\rho_s C_{p,s} + M_w C_{p,wl} n_{wl}\right) \overline{u}_0 \bullet \nabla T_{sl} + \frac{\kappa}{\alpha_s} T_{sl} = \frac{\kappa}{\alpha_s} T_{sl} - Q_v - Q_{v,bc} - Q_{\Delta T} + Q_{RF} \tag{48}$$

B.3. Gas and vapor temperature

The sensible enthalpy of the gas/vapor domain is the sum of the sensible enthalpy of water vapor and air,

$$H_{s,av} = T_{av}\left(M_w C_{p,wv} n_{wv} + M_a C_{p,a} n_a\right) \tag{49}$$

The local heat balance in the gas/vapor domain, accounting for conduction of heat, convection of heat, and heat transfer from the solid/liquid phase domain is expressed as follows,

$$\partial_t H_{s,av} = \kappa_{av} \nabla^2 T_{av} - M_w C_{p,wv}\left(T_{av} n_{wv} \nabla \bullet \overline{u}_{av} + n_{wv} \nabla T_{av} \bullet \overline{u}_{av} + T_{av} \nabla n_{wv} \bullet \overline{u}_{av}\right) - M_a C_{p,a}\left(T_{av} n_a \nabla \bullet \overline{u}_{av} + n_a \nabla T_{av} \bullet \overline{u}_{av} + T_{av} \nabla n_a \bullet \overline{u}_{av}\right) + r_v M_w C_{p,wv} T_{av} + Q_{\Delta T} \tag{50}$$

The time derivative of the sensible enthalpy (Eq. (49) is,

$$\partial_t H_{s,av} = \partial_t T_{av}\left(M_w C_{p,wv} n_{wv} + M_a C_{p,a} n_a\right) + T_{av}\left(M_w C_{p,wv} \partial_t n_{wv} + M_a C_{p,a} \partial_t n_a\right) \tag{51}$$

Substituting Eq. (50), 56 and 57 (Section B.4), into Eq. (51), and neglecting the α_v diffusion terms that cancel out by approximation yields,

$$\begin{aligned}&\partial_t T_{av}\left(M_w C_{p,wv} n_{wv} + M_a C_{p,a} n_a\right) + T_{av}\left(M_w C_{p,wv}\left(-n_{wv}\nabla \bullet \overline{u}_{av} - \overline{u}_{av} \bullet \nabla n_{wv} + r_v\right) + M_a C_{p,a}\left(-n_a \nabla \bullet \overline{u}_{av} - \overline{u}_{av} \bullet \nabla n_a\right)\right)\\ &= \kappa_{av}\nabla^2 T_{av} - M_w C_{p,wv}\left(T_{av} n_{wv}\nabla \bullet \overline{u}_{av} + n_{wv}\nabla T_{av} \bullet \overline{u}_{av} + T_{av}\nabla n_{wv} \bullet \overline{u}_{av}\right) - M_a C_{p,a}\left(T_{av} n_a \nabla \bullet \overline{u}_{av} + n_a \nabla T_{av} \bullet \overline{u}_{av} + T_{av}\nabla n_a \bullet \overline{u}_{av}\right) + r_v M_w C_{p,wv} T_{av} + Q_{\Delta T}\end{aligned} \tag{52}$$

Elimination of terms left and right of the equal sign, substituting Eq. (58) from Section B.4 and Eq. (8) from Section 4.2, and rearrangement results in,

$$\partial_t T_{av}\left(M_w C_{p,wv} n_{wv} + M_a C_{p,a} n_a\right) = \kappa_{av}\nabla^2 T_{av} + \left(M_w C_{p,wv} n_{wv} + M_a C_{p,a} n_a\right)\nabla T_{av} \bullet \left(\frac{k}{\mu\varphi}\nabla p - \overline{u}_0\right) + \left(M_w C_{p,wv} n_{wv} + M_a C_{p,a} n_a\right)\left(T_{sl} - T_{av}\right)\frac{1}{\tau_v} \tag{53}$$

which is rearranged into,

$$\left(M_w C_{p,wv} n_{wv} + M_a C_{p,a} n_a\right)\partial_t T_{av} + \nabla \bullet -\kappa_{av}\nabla T_{av} + \left(M_w C_{p,wv} n_{wv} + M_a C_{p,a} n_a\right)\left(\frac{k}{\mu\varphi}\nabla p - \overline{u}_0\right) \bullet \nabla T_{av} + \frac{M_w C_{p,wv} n_{wv} + M_a C_{p,a} n_a}{\tau_v} T_{av} = \frac{M_w C_{p,wv} n_{wv} + M_a C_{p,a} n_a}{\tau_v} T_{sl} \tag{54}$$

B.4. Gas and vapor pressure

The ideal gas law relates pressure, molar bulk densities of air and vapor, and temperature as follows,

$$p\varphi = \left(n_{wv} + n_a\right) R T_{av} \approx \left(n_{wv} + n_a\right) R T_{sl} \tag{55}$$

Note that the porosity is included in his equation. Moreover, the solid/liquid temperature is used as an approximation for the gas/vapor temperature because this improves convergence. The local mass balance for water vapor over a control volume is,

$$\partial_t n_{wv} = \alpha_v \nabla^2 n_{wv} - n_{wv}\nabla \bullet \overline{u}_{av} - \overline{u}_{av} \bullet \nabla n_{wv} + r_v \tag{56}$$

For air a similar equation is defined. The diffusion term $\alpha_v \nabla^2 n_{wv}$ recurs here since water vapor that is transported through diffusion is displaced by air,

$$\partial_t n_a = -\alpha_v \nabla^2 n_{wv} - n_a \nabla \bullet \overline{u}_{av} - \overline{u}_{av} \bullet \nabla n_a \tag{57}$$

The symbol $\overline{u}_{av}$ represents the flow velocity of gas and vapor in soil. This velocity is the sum of the imposed advection velocity, and the velocity of flow in porous media due to pressure variation according to Darcy's Law,

$$\overline{u}_{av} = -\frac{k}{\mu\varphi}\nabla p + \overline{u}_0 \tag{58}$$

Differentiation of Eq. (55) to time yields,

$$\varphi\partial_t p = \left(\partial_t n_{wv} + \partial_t n_a\right) R T_{sl} + \left(n_{wv} + n_a\right) R \partial_t T_{sl} \tag{59}$$

and substitution of Eqs. (55)–(58) into Eq. (59) yields,

$$\begin{aligned}\varphi\partial_t p = &\left[\left(\alpha_v \nabla^2 n_{wv} + \frac{k}{\mu\varphi} n_{wv}\nabla^2 p + \nabla n_{wv} \bullet \left(\frac{k}{\mu\varphi}\nabla p - \overline{u}_0\right) + r_v\right) + \left(-\alpha_v \nabla^2 n_{wv} + \frac{k}{\mu\varphi}\left(\frac{p\varphi}{RT_{sl}} - n_{wv}\right)\nabla^2 p + \nabla\left(\frac{p\varphi}{RT_{sl}} - n_{wv}\right) \bullet \left(\frac{k}{\mu\varphi}\nabla p\right.\right.\right.\\ &\left.\left.\left. - \overline{u}_0\right)\right)\right] R T_{sl} + \left[n_{wv} + \left(\frac{p\varphi}{RT_{sl}} - n_{wv}\right)\right] R \partial_t T_{sl}\end{aligned} \tag{60}$$

Simplifying and applying the quotient rule $\left(\nabla\left(\frac{f}{g}\right) = \frac{g\nabla f - f\nabla g}{g^2}\right)$ yields,

$$\varphi\partial_t p = \left[\frac{k}{\mu}\frac{p}{T_{sl}}\nabla^2 p + \varphi\frac{T_{sl}\nabla p - p\nabla T_{sl}}{{T_{sl}}^2} \bullet \left(\frac{k}{\mu\varphi}\nabla p - \overline{u}_0\right) + R r_v\right] T_{sl} + \frac{p\varphi}{T_{sl}}\partial_t T_{sl} \tag{61}$$

which is rearranged to bring the equation into the form of Eq. (35),

$$\partial_t p + \nabla \bullet -\frac{k\widehat{p}}{\mu\varphi}\nabla p + \left(\frac{kp}{\mu\varphi}\frac{\nabla T_{sl}}{T_{sl}} + \overline{u}_0 - \frac{k}{\mu\varphi}\nabla\widehat{p}\right) \bullet \nabla p - \left(\frac{\nabla T_{sl}}{T_{sl}} \bullet \overline{u}_0 + \frac{\partial_t T_{sl}}{T_{sl}}\right) p = \frac{T_{sl} R}{\varphi} r_v \tag{62}$$

B.5. Water vapor bulk density

The mass balance accounting respectively for the diffusion of water in air, the convection of water vapor with pressure driven flow, and the evaporation and condensation between the solid/liquid domain and gas/vapor domain is,

$$\partial_t n_{wv} = \alpha_v \nabla^2 n_{wv} - n_{wv}\nabla \bullet \overline{u}_{av} - \overline{u}_{av} \bullet \nabla n_{wv} + r_v \tag{63}$$

Substitution of the velocity expression for flow of gas and vapor (Eq. (58) and rearranging yields,

$$\partial_t n_{wv} + \nabla \bullet -\alpha_v \nabla n_{wv} - \left(\frac{k\nabla p}{\mu\varphi} - \overline{u}_0\right) \bullet \nabla n_{wv} - \frac{k\nabla^2 p}{\mu\varphi} n_{wv} = r_v \tag{64}$$

Appendix C. Derivation of boundary equation expressions.

This appendix details derivations of formulations that are used to describe boundary conditions for the transport phenomena at the edge of the soil domain. In Section C.1 the boundary condition for pressure at the boundary adjacent to soil outside of the simulated soil volume is determined. In Section C.2 the characteristic length is calculated of the interaction due to evaporation between soil volume and the ambient air above it. In Section C.3 the heat and mass transfer coefficients due to natural convection are calculated at the top plane boundary between soil and ambient air.

C.1. Pressure boundary condition adjacent to soil

The pressure variations in soil outside of the simulated soil volume cannot be neglected. However, it is undesired to extend the size of this volume so that the pressure variations would approximate zero at its boundaries, because this would likely increase of the computational requirements beyond the practical constraints on computational hardware that are imposed in the scope of this work.

An alternative approach is applied, in which a boundary condition description is developed that approximates the behavior of a soil domain beyond the boundary. These are needed only in the boundaries that are parallel with the direction of motion of the soil volume relative to the antenna. To this end, it is assumed 1) that the flow beyond these planes extends into an infinite domain; 2) that this flow only occurs in the direction perpendicular to these planes, i.e. it is a one-dimensional flow; 3) that the effect decays and approaches zero with increasing distance to the plane; and 4) that pressure does not deviate much from the ambient pressure.

A spatial coordinate w is introduced that is the distance perpendicular to the boundary plane in an outward direction. The relation between flow and pressure follows from Darcy's law,

$$u_w = -\frac{k}{\mu\varphi}\partial_w p \tag{65}$$

The ideal gas law determines the relation between the molar bulk density of gas and vapor, and pressure,

$$n = p\frac{\varphi}{RT} \tag{66}$$

The mass balance for air and water vapor combined is,

$$\partial_t n = -n\partial_w u_w - u_w\partial_w n \tag{67}$$

Substitution of Eq. (65) and (66) into Eq. (67) yields,

$$\partial_t p = \frac{k}{\mu\varphi}(\partial_w p)^2 + \frac{k}{\mu\varphi}\partial_w^2(p)p \tag{68}$$

With the assumption that pressure does not deviate much from the ambient pressure, Eq. (68) can be simplified as follows,

$$\partial_t \tilde{p} = p_0\frac{k}{\mu\varphi}\partial_w^2(\tilde{p}) \tag{69}$$

in which $\tilde{p}$ represents the pressure variations relative to the ambient pressure,

$$\tilde{p} = p - p_0 \tag{70}$$

The differential equation is solved via separation of variables,

$$\tilde{p}(w,t) = W(w)V(t) \tag{71}$$

$$W(w)V'(t) = \frac{p_0 k}{\mu\varphi}W''(w)V(t) \tag{72}$$

$$\frac{V'(t)}{V(t)} = \frac{p_0 k}{\mu\varphi}\frac{W''(w)}{W(w)} = C_0 \tag{73}$$

To find a fitting solution, a time harmonic approximation is applied to account for time-dependence. Preliminary simulation has shown that a radial frequency $\omega_{bc} = 0.01$ rad/s characterizes the dynamics at the boundaries. This defines coefficient C_0 as follows,

$$V(t) = C_1\exp(i\omega_{bc}t) \tag{74a}$$

$$V'(t) = i\omega_{bc}C_1\exp(i\omega_{bc}t) \tag{74b}$$

$$C_0 = i\omega_{bc} \tag{74c}$$

Coefficient C_0 must therefore be an imaginary number. A fitting solution is found as follows,

$$W(w) = C_2\exp\big(-(1+i)\gamma_p w\big) \tag{75a}$$

$$W''(w) = (1+i)^2\gamma_p{}^2 C_2\exp\big(-(1+i)\gamma_p w\big) \tag{75b}$$

$$C_0 = \frac{p_0 k}{\mu\varphi}(1+i)^2\gamma_p{}^2 = \frac{p_0 k}{\mu\varphi}2i\gamma_p{}^2 \tag{75c}$$

Hence,

$$i\omega_{bc} = \frac{p_0 k}{\mu\varphi} 2i{\gamma_p}^2$$

$$\gamma_p = \sqrt{\frac{\mu\varphi\omega_{bc}}{2p_0 k}} \tag{76}$$

and the function that fits differential equation Eq. (69) is,

$$\widetilde{p}(w,t) = C_3 \exp\left(i\omega_{bc}t - (1+i)\sqrt{\frac{\mu\varphi\omega_{bc}}{2p_0 k}}w\right) \tag{77}$$

Combining this pressure expression with Darcy's law (Eq. (65) yields,

$$u_w(w,t) = (1+i)\sqrt{\frac{k\omega_{bc}}{2p_0\mu\varphi}} C_3 \exp\left(i\omega_{bc}t - (1+i)\sqrt{\frac{\mu\varphi\omega_{bc}}{2p_0 k}}w\right)$$

$$u_w(w,t) = \sqrt{\frac{k\omega_{bc}}{2p_0\mu\varphi}}\widetilde{p} + i\omega_{bc}\sqrt{\frac{k}{2p_0\mu\varphi\omega_{bc}}}\widetilde{p} \tag{78}$$

Which corresponds to the following differential equation under the assumption of a time harmonic variation,

$$u_w(w,t) = \sqrt{\frac{k\omega_{bc}}{2p_0\mu\varphi}}\widetilde{p}(w,t) + \sqrt{\frac{k}{2p_0\mu\varphi\omega_{bc}}}\partial_t\widetilde{p}(w,t) \tag{79}$$

Reintroducing absolute pressure (Eq. (70), substituting Darcy's Law (Eq. (65), and using the pressure gradient in the soil volume multiplied with the speed of motion of the antenna as an expression for the time derivative of pressure yields,

$$-\frac{k}{\mu\varphi}\partial_w p = \sqrt{\frac{k\omega_{bc}}{2p_0\mu\varphi}}(p - p_0) + \sqrt{\frac{k}{2p_0\mu\varphi\omega_{bc}}}u_0\partial_x p \tag{80}$$

This differential equation describes the boundary condition for pressure at the boundaries of the soil volume that are adjacent to soil. Specifically, this relates to the boundaries at the bottom and side planes of the soil volume as defined in Fig. 2. Two subsequent operations are applied to bring the equation in the form required by the PDE interface of Comsol Multiphysics for flux boundary conditions. First the spatial derivative in the w-direction is expressed as the inner product of the pressure gradient inside the soil volume with the normal vector $\overline{n}$ of the boundary plane. Second, the equation is multiplied by pressure. The assumption is made herein that at the boundary, the pressure does not deviate much from the ambient pressure. The expression for the boundary condition becomes,

$$-\overline{n}\bullet -\frac{\widehat{p}k}{\mu\varphi}\nabla p = -\sqrt{\frac{p_0 k\omega_{bc}}{2\mu\varphi}}(p - p_0) - \sqrt{\frac{p_0 k}{2\mu\varphi\omega_{bc}}}u_0\partial_x p \tag{81}$$

C.2. Characteristic length of soil/air interaction layer

The boundary conditions related to evaporation and condensation of moisture between soil and ambient air are represented by a volumetric source/sink term. An interaction layer in soil is defined directly below the top boundary plane where this transfer of moisture takes place. In this layer, a distribution function is applied that decays with depth, and that describes the distribution of the influence of transfer of moisture to and from ambient air.

In order to define this distribution function, a characteristic length is calculated. Of the relevant diffusion processes at play, thermal diffusion and vapor diffusion have the most significant diffusivities by an order of magnitude, so it is assumed that the characteristic length is determined by these two processes. Moreover, it is assumed that the soil top layer is at the vapor–liquid thermodynamic equilibrium; and that the gas/vapor pressure equals ambient pressure. The transport parameters are calculated for an approximate average temperature of 40 °C and a soil moisture level corresponding to 21.5 m%.

The volumetric heat capacity of soil under these conditions is $\rho_{sl}C_{p,sl} = 4568\ \mathrm{kJ/m^3K}$; the enthalpy of evaporation is $H_v M_w = 43339\ \mathrm{kJ/mol}$; and the temperature derivative of the volumetric molar bulk density of water vapor at equilibrium is $\partial_T n_{wv} = \partial_T\left(\frac{\varphi}{R}\frac{f_A(T)}{T}\right) = \frac{\varphi}{R}\frac{f_A - f_A/T}{T} = 7.1115\,\frac{\mathrm{mmol}}{\mathrm{m^3}}\,\frac{1}{\mathrm{K}}$. The diffusion and evaporation/condensation processes are represented by the following equations,

$$\partial_t n_{wv} = \alpha_v\nabla^2 n_{wv} + r_v \tag{82}$$

$$\partial_t n_{wl} = -r_v \tag{83}$$

$$\partial_t T = -\frac{H_v M_w}{\rho_{sl}C_{p,sl}}r_v + \frac{\kappa}{\rho_{sl}C_{p,sl}}\nabla^2 T \tag{84}$$

$$\partial n_{wv} = \partial_T n_{wv}\partial T \tag{85}$$

Substituting Eqs. (83) and (85) into Eq. (84) and rearranging results in,

$$\partial_t n_{wl} = \frac{\rho_{sl}C_{p,sl}}{H_v M_w \partial_T n_{wv}}\partial_t n_{wv} - \frac{\kappa}{H_v M_w \partial_T n_{wv}}\nabla^2 n_{wv} \tag{86}$$

Substituting Eq. (83) into Eq. (82) yields,

$$\partial_t n_{wl} = \alpha_v \nabla^2 n_{wv} - \partial_t n_{wv} \tag{87}$$

Combining Eqs. (86) and (87) by equating $\partial_t n_{wl}$ results in an expression for a combined diffusivity,

$$\partial_t n_{wv} = \frac{\alpha_v + \frac{\kappa}{H_v M_w \partial_T n_{wv}}}{\frac{\rho_{sl} C_{p,sl}}{H_v M_w \partial_T n_{wv}} + 1} \nabla^2 n_{wv} = \alpha_{combi} \nabla^2 n_{wv} \tag{88}$$

The combined diffusivity is,

$$\alpha_{combi} = \frac{2.8 \bullet 10^{-5} + 6.49 \bullet 10^{-3}}{14.8 \bullet 10^{3} + 1} = 4.4 \bullet 10^{-7}\ \mathrm{m^2}\Big/\mathrm{s}$$

The depth of the interaction layer is calculated by imposing a time-harmonic function with the same radial frequency $\omega_{bc} = 0.01$ rad/s as is used in Section C.1,

$$n_{wv}(z,t) = C_4 e^{\gamma_p z} e^{i\omega_{bc} t} \tag{89}$$

Substitution of Eq. (89) into the differential equation for diffusion (Eq. (88) allows for the calculation of the characteristic depth of the soil/air interaction layer L_s,

$$i\omega_{bc} = \alpha_{combi} {\gamma_s}^2$$

$$\gamma_s = \frac{1+i}{\sqrt{2}} \sqrt{\frac{\omega_{bc}}{\alpha_{combi}}}$$

$$L_s = \mathrm{Re}(\gamma_s)^{-1} = \sqrt{\frac{2\alpha_{combi}}{\omega_{bc}}} = 9.4\ \mathrm{mm}$$

Following this analysis the interaction layer has a characteristic length of 9.4 mm, or approximately 10 mm.

C.3. Convective heat and mass transfer coefficients at the top plane boundary

Natural convection determines the rate of heat transfer and evaporation between the top soil surface and ambient air. The natural convection coefficient for heat transfer is determined first. This is done according to Mills (1999) who cites McAdams (1954) on the matter. The calculation first determines the Rayleigh number for a characteristic length L of 0.4 m – defined to be the width of the antenna in the model – and a temperature difference ΔT of 40 °C, which is approximately half the maximum surface temperature rise,

$$\mathrm{Ra} = \frac{\rho \beta \Delta T L^3 g}{\mu \alpha} \tag{90}$$

The air properties applied here are: a density ρ of 1.25 kg/m^3, thermal expansion coefficient β of 3.6·10^{-3} 1/K, gravitational acceleration g of 9.81 m/s^2, dynamic viscosity μ of 1.7·10^{-5} Pa·s, and thermal diffusivity α of 1.9·10^{-5} m^2/s. The Rayleigh number is calculated to be 3.32·10^8, which directs to the following relation as appropriate to calculate the Nusselt number,

$$\mathrm{Nu} = 0.14 Ra^{1/3} \tag{91}$$

This results in a value of 96.9. The convection coefficient is calculated from the Nusselt number with a thermal conductivity for air of 2.5·10^{-2} W/(mK),

$$\mathrm{Nu} = \frac{h_{n,T} L}{\kappa} \tag{92}$$

The convection coefficient is calculated to be 6.1 W/(m^{2}K). The properties for air are obtained from several Engineering Toolbox pages (2003a) (2003b) (2018) (2009).

Next, the natural convection coefficient for mass transfer is calculated, based on the analogy between heat and mass transfer (Mills, 1999) (Kays & Crawford, 1993). The analogue of the Nusselt number is the Sherwood number. As the Rayleigh number is the product of the Grashof number and the Prandtl number, it follows that substituting the product of Grashof number and Schmidt number into Eq. (91) yields the Sherwood number,

$$\mathrm{Sh} = 0.14(\mathrm{GrSc})^{1/3} = 0.14\left(Ra \frac{\mathrm{Sc}}{\mathrm{Pr}}\right)^{1/3} \tag{93}$$

The resulting Sherwood number is 90.8. From the equation for the Sherwood number, the convective mass transfer coefficient is derived,

$$\mathrm{Sh} = \frac{h_{n,m}}{\alpha_v / L} \tag{94}$$

The resulting mass transfer coefficient is $h_{n,m} = 6.36$ mm/s.

Appendix D. Notes on complex dielectric medium properties

The dielectric medium properties are a key aspect of the radio wave treatment process. However, they are uncommon to both the disciplinary fields of biology and transport phenomena. This may lead to misunderstandings with respect to the nature of dielectric properties. Therefore, in this appendix some notes are included to mitigate these misunderstandings in case they occur.

First, there is the manner in which the dielectric properties are defined. They are defined in the frequency domain, instead of the intuitively more

accessible time domain. This stems from the mathematical convenience of converting Maxwell's electromagnetic field equations from the time domain to a frequency domain representation. The time domain representation can be expressed as follows,

$$\begin{aligned} \nabla \times \mathbf{E} &= -\partial_t \mu \mathbf{H} \\ \nabla \times \mathbf{H} &= \partial_t \varepsilon \mathbf{E} + \mathbf{J} \end{aligned} \tag{95}$$

In these differential equations **E** is the electric field vector and **H** is the magnetic field vector, **J** is the vector for the excitation current. Also present in these equations is a time derivative operator ∂_t, which signifies that the differential equations describe a process that varies in time, and hence it is a representation of the process in the time domain. Electromagnetic fields, however, are typically considered as stationary at a single frequency. For example, in the case of radio wave treatment of soil, this frequency is 915 MHz. This allows for a modification of these differential equation by imposing a sinusoidally oscillating solution at a single frequency for the electromagnetic field solutions. Specifically, the sinusoidally oscillating field, also known as a time-harmonic field has the following general form,

$$\mathbf{V}(t,x) = e^{i\omega t}\mathbf{V}(x) \tag{96}$$

In this expression **V** is an arbitrary vector variable. By imposing this solution, an algebraic relation can be used for the time derivative of the vector fields, i.e. $\partial_t \mathbf{V} = i\omega \mathbf{V}$, where ω represents the angular frequency of the excitation. The angular frequency is the regular frequency multiplied by 2π, e.g. for the soil treatment process the applied frequency is 915 MHz, and the angular frequency equals $2\pi \cdot 915 \cdot 10^6 = 5.749 \cdot 10^9$ rad/s. By imposing a time–harmonic field solution, the following modification to Maxwell's electromagnetic field equations results,

$$\begin{aligned} \nabla \times \mathbf{E} &= -i\omega \mu \mathbf{H} \\ \nabla \times \mathbf{H} &= i\omega \varepsilon \mathbf{E} \end{aligned} \tag{97}$$

Note that the excitation current **J** is not included in these expressions. This modification brings Maxwell's equations into the frequency domain. This has several advantages. First, it allows for calculation for just one frequency of interest. All other non-relevant dynamic behavior is avoided, which is considerably more efficient computationally. Second, it also requires consideration of medium properties at just one frequency, which greatly reduces the required effort in medium properties measurement. The consequence of the shift to the frequency domain is the introduction of complex–valued variables. From an everyday perspective this may appear non-intuitive, but that does not weigh up to the conveniences in terms of computational requirements and medium properties measurement.

The introduction of complex–valued variables extends to the medium properties, which explains the typical representation of the dielectric properties in the form $\varepsilon' - i\varepsilon''$. These dielectric properties define the microscopic polarization of charge inside a medium in response to the application of an electric field vector **E**. The aforementioned form is a simplification; a more comprehensive expression would be,

$$\varepsilon(\omega, T) = \varepsilon_0 \varepsilon_r(\omega, T) = \varepsilon_0(\varepsilon'(\omega, T) - i\varepsilon''(\omega, T)) \tag{98}$$

This formula shows how the symbol ε is used to express the various definitions of the dielectric properties. These properties are also called the *dielectric permittivity*, or just *permittivity*. Commonly these properties are expressed as the *relative permittivity*, denoted by the symbol ε_r; in that case, the permittivity is expressed relative to the permittivity of vacuum, $\varepsilon_0 = 8.8542(\ldots) \cdot 10^{-12}$F/m. The convenience lies in the removal of the long number of decimals and the order of magnitude term. The relative permittivity is thus expressed in more manageable dimensionless numbers, which ranges for everyday media in absolute values from 1 for vacuum to about 80 for water.

For lossy materials, as encountered in applications where exposure of a medium to an electromagnetic field causes heating, the relative permittivity is complex valued. This is often expressed in the aforementioned form $\varepsilon_r = \varepsilon' - i\varepsilon''$. In this expression, the real part ε' quantifies the electric energy stored in a medium due to microscopic charge polarization upon exposure to the electric field vector, while the imaginary ε'' part quantifies the dissipation of electric energy into heat.

It must be noted here, though, that this form is a simplification. As Eq. (98) shows, both the real and imaginary parts of the relative permittivity can be a function of both frequency and temperature. For composite media, such as soil, the relative permittivity is a function of its composition as well. A dielectric properties measurement at one particular frequency or temperature *can never a priori be assumed* to apply at a different frequency or temperature. This holds in particular for medium properties determined for static or quasi-static fields versus fields in ultra–high frequency bands (UHF, 0.3–3 GHz). Some media such as glasses and other ceramics are relatively invariant, water and organic liquids are typically highly dependent. On a final note, for completeness, non–isotropic properties of media may need to be considered, which for example might possibly be induced in soils by a dominant direction of root growth.

The imaginary part ε'' – also known as the dielectric loss term – lumps purely dielectric heating and conductive heating into a singular term. Colloquially this form of heat generation is often referred to as dielectric heating, but conductive heating may be lumped in with it as well. The former heating mechanism is caused by impeded rotation of polar species, while the latter is caused by impeded translation of electrically charged species. Expressions can be defined in which a distinction is made between the separate dissipation mechanisms, e.g. Eq. (25). A clear distinction between the mechanisms cannot be made, however, when only a single measurement is made at one particular frequency. In contrast, a spectral measurement over a wide frequency band may enable distinction between dissipation mechanisms.

For the application that forms the context of this study, i.e. radio wave treatment of soil, only heat generation through dissipation of the electric field vector is considered. Magnetic dissipation is presumed not to occur. Therefore, the magnetic permeability μ is set to the permeability of vacuum $\mu_0 = 4\pi \cdot 10^{-7}$H/m throughout the study. Magnetic dissipation may occur, though, in case the soil under consideration has particular magnetic properties. In that case, the mathematical expressions for the magnetic properties of media are largely analogue to the dielectric properties.

References

Abbey, L., Udenigwe, C., Mohan, A., Anom, E., 2017. Microwave irradiation effects on vermicasts potency, and plant growth and antioxidant activity in seedlings of Chinese cabbage (Brassica rapa subsp. pekinensis). J. Radiat. Res. Appl. Sci. 10, 110–116. https://doi.org/10.1016/j.jrras.2017.01.002.

Agro Energy, 2017. *De elektriciteitsmarkt in vogelvlucht in de tuinbouw.* [Online] Available at: https://www.agro-energy.nl/wp-content/uploads/2017/03/Whitepaper_Energiemarkt_in_vogelvlucht_LR.pdf[Accessed 9 3 2020].

Bear, J., 1972. Dynamics of fluids in porous media. Dover Publications, New York.

Bollen, G., 1969. The selective effect of heat treatment on the microflora of a greenhouse soil. Neth. J. Plant Pathol. 75, 157–163. https://doi.org/10.1007/BF02137211.

Brodie, G., et al., 2015. Assessing the Impact of Microwave Treatment on Soil Microbial Populations. Global Journal of Agricultural Innovation, Research & Development 2 (1), 25–32. https://doi.org/10.15377/2409-9813.2015.02.01.3.

Brodie, G., Khan, M. & Gupta, D., 2020. Microwave Soil Treatment and Plant Growth. In: M. Hasanuzzaman, M. Fujita, M. Teixeira Filho & T. Nogueira, eds. *Sustainable Crop Production.* London: InTechOpen, https://doi.org/10.5772/intechopen.89684.

Brodie, G., Ryan, C., Lancaster, C., 2012. Microwave Technologies as Part of an Integrated Weed Management Strategy: A Review. Int. J. Agronomy, 636905. https://doi.org/10.1155/2012/636905.

Chen, Y., Gamliel, A., Stapleton, J., Aviad, T., 1991. Chemical, Physical, and Microbial Changes Related to Plant Growth in Disinfested Soil. In: Katan, J., DeVay, J. (Eds.), Soil Solarization. CRC Press, Boca Raton.

COMSOL AB, COMSOL Multiphysics 5.5 2019 Stockholm.

Conchado, A., Linares, P., 2012. The Economic Impact of Demand-Response Programs on Power Systems. A Survey of the State of the Art. In: Sorokin, A. (Ed.), Handbook of Networks In Power Systems I. Energy Systems. Heidelberg, Berlin.

Dabbene, F., Gay, P., Tortia, C., 2003. Modelling and Control of Steam Soil Disinfestation Processes. Biosyst. Eng. 84 (3), 247–256. https://doi.org/10.1016/S1537-5110(02)00276-3.

European Parliament and Council, 2013. *Directive 2013/35/EU on the minimum health and safety requirements regarding the exposure of workers to the risks arising from physical agents (electromagnetic fields).* [Online] Available at: https://eur-lex.europa.eu/legal-content/en/TXT/PDF/?uri=CELEX:32013L0035[Accessed 13 1 2022].

Ferriss, R., 1984. Effects of Microwave oven treatment on microorganisms in soil. Phytopathology 74 (1), 121–126. https://www.doi.org/10.1094/Phyto-74-121.

Fujikawa, H., Itoh, T., 1998. Thermal Inactivation Analysis of Mesophiles Using the Arrhenius and z-Value Models. J. Food Prot. 61 (7), 910–912. https://doi.org/10.4315/0362-028X-61.7.910.

Griffin, G., Baker, R., 1991. Population Dynamics of Plant Pathogens and Associated Organisms in Soil in Relation to Infectious Inoculum. In: Katan, J., DeVay, J. (Eds.), Soil Solarization. CRC Press, Boca Raton.

Henry P., The diffusion of moisture and heat through textiles. Discussions of the Faraday Society 1948 10.1039/DF9480300243 243 257.

International Telecommunication Union, 2020. *Radio Regulations.* [Online] Available at: https://www.itu.int/dms_pub/itu-r/opb/reg/R-REG-RR-2020-ZPF-E.zip[Accessed 19 9 2022].

Kaatze, U., 1989. Complex Permittivity of Water as a Function of Frequency and Temperature. J. Chem. Eng. Data 34, 371–374. https://doi.org/10.1021/je00058a001.

Katan, J., DeVay, J. (Eds.), 1991a. Soil Solarization. CRC Press, Boca Raton.

Katan, J., DeVay, J., 1991b. Soil Solarization: Historical Perspectives, Principles, and Uses. In: Katan, J., DeVay, J. (Eds.), Soil Solarization. CRC Press, Boca Raton.

Kays, W., Crawford, M., 1993. Convective heat and mass transfer, 3rd ed. McGraw-Hill, New York.

Khan, M., Brodie, G., Gupta, D., 2016. Effect of microwave (2.45 GHz) treatment of soil on yield components of wheat (Triticum aestivum L.). J. Microw. Power Electromagn. Energy. 50 (3), 191–200. https://doi.org/10.1080/08327823.2016.1228441.

King Hubbert, M., 1956. Darcy's Law and the Field Equations of the Flow of Underground Fluids. AIME Petroleum Transactions 207 (1), 222–239. https://doi.org/10.2118/749-G.

Koppert Machines, 2014. *20140327 koppertmachines agritron.* [Online] Available at: https://www.youtube.com/watch?v=Rdk4JZnOKig[Accessed 24 1 2020].

Kremer, E., Schönhals, A. (Eds.), 2003. Broadband Dielectric Spectroscopy. Springer-Verlag, Berlin.

Mahdi, W., Al-Badri, K., Alqaisi, M., 2021. Effect of Microwave Radiation on Bacteria, Fungi and Some Growth Characteristics of Cowpea Vigna unguiculata L. *Gesunde Pflanzen*, Issue 73, 161–167. https://doi.org/10.1007/s10343-020-00534-2.

The Mathworks, 2019. MATLAB, R2019b. Natrick.

McAdams, W., 1954. Heat Transmission, 3rd ed. McGraw-Hill, New York.

Meredith, R., 1998. Engineers' Handbook of Industrial Microwave Heating. Institution of Electrical Engineers, London.

Miler, N., Kulus, D., 2018. Microwave treatment can induce chrysanthemum phenotypic and genetic changes. *Sci. Hortic.*, Issue 227, 223–233. https://doi.org/10.1016/j.scienta.2017.09.047.

Mills, A., 1999. Basic Heat & Mass Transfer, 2nd ed. Prentice-Hall, New Jersey.

Nelson, S., 1996. A review and assessment of microwave energy for soil treatment to control pests. Transactions of the ASAE 39 (1), 281–289. https://doi.org/10.13031/2013.27508.

NIST Chemistry Webbook, 2018. *Water.* [Online] Available at: https://webbook.nist.gov/cgi/cbook.cgi?ID=C7732185&Units=SI&Mask=4#Thermo-Phase[Accessed 5 2 2020].

Peleg, M., Normand, M., Corradini, M., 2012. The Arrhenius Equation Revisited. Crit. Rev. Food Sci. Nutr. 52, 830–851. https://doi.org/10.1080/10408398.2012.667460.

Polle, A., Chen, S., 2015. On the salty side of life: molecular, physiological and anatomical adaptation and acclimation of trees to extreme habitats. Plant Cell Environ. 38, 1794–1816. https://doi.org/10.1111/pce.12440.

Pozar, D., 2005. Microwave Engineering, 3rd ed. Wiley, Hoboken.

Pullman, G., DeVay, J., Garber, R., 1981. Soil Solarization and Thermal Death—A Logarithmic Relationship Between Time and Temperature for Four Soilborne Pathogens. Phytopathology 71 (9), 954–959. https://doi.org/10.4315/0362-028X-61.7.910.

Radoiu, M., 2011. *personal communication* [Interview] (25 1 2011).

Rasing, F. & Jansen, W., 2007. *Diëlektrisch ontsmetten van substraten - Een goed alternatief voor stromen?.* [Online] Available at: https://edepot.wur.nl/117179[Accessed 9 3 2020].

Rasing, F. & Jansen, W., 2010. *Diëlektrisch ontsmetten van kasgrond - Een goed alternatief voor stomen?.* [Online] Available at: https://edepot.wur.nl/287611[Accessed 9 3 2020].

Roux-Michollet, D., Dudal, Y., Jocteur-Monrozier, L., Czarnes, S., 2010. Steam treatment of surface soil: how does it affect water-soluble organic matter, C mineralization, and bacterial community composition? Biol. Fertil. Soils 46, 607–616. https://doi.org/10.1007/s00374-010-0468-6.

Sihvola, A., 1999. Electromagnetic mixing formulas and applications. The Institution of Electrical Engineers, London.

Staalduinen, J. v., 2022. *Kan rijdende magnetron het stomen vervangen in grondteelten?.* [Online] Available at: https://www.onderglas.nl/kan-rijdende-magnetron-het-stomen-vervangen-in-grondteelten/[Accessed 14 4 2023].

Staple, W., 1965. Moisture tension, diffusivity, and conductivity of a loam soil during wetting and drying. Can. J. Soil Sci. 45, 78–86. https://doi.org/10.4141/cjss65-010.

The Engineering Toolbox, 2003a. *Air - Density, Specific Weight and Thermal Expansion Coefficient at Varying Temperature and Constant Pressures.* [Online] Available at: https://www.engineeringtoolbox.com/air-density-specific-weight-d_600.html[Accessed 16 3 2020].

The Engineering Toolbox, 2003b. *Air - Dynamic and Kinematic Viscosity.* [Online] Available at: https://www.engineeringtoolbox.com/air-absolute-kinematic-viscosity-d_601.html[Accessed 5 2 2020].

The Engineering Toolbox, 2003c. *Air - Thermophysical Properties.* [Online] Available at: https://www.engineeringtoolbox.com/air-properties-d_156.html[Accessed 5 2 2020].

The Engineering Toolbox, 2003d. *Water - Thermophysical Properties.* [Online] Available at: https://www.engineeringtoolbox.com/water-thermal-properties-d_162.html [Accessed 5 2 2020].

The Engineering Toolbox, 2004a. *Air - Molecular Weight and Composition.* [Online] Available at: https://www.engineeringtoolbox.com/molecular-mass-air-d_679.html [Accessed 5 2 2020].

The Engineering Toolbox, 2004b. *Air - Specific Heat at Constant Pressure and Varying Temperature.* [Online] Available at: https://www.engineeringtoolbox.com/air-specific-heat-capacity-d_705.html[Accessed 5 2 2020].

The Engineering Toolbox, 2004c. *Steam Viscosity.* [Online] Available at: https://www.engineeringtoolbox.com/steam-viscosity-d_770.html[Accessed 5 2 2020].

The Engineering Toolbox, 2005. *Water Vapor - Specific Heat.* [Online] Available at: https://www.engineeringtoolbox.com/water-vapor-d_979.html[Accessed 5 2 2020].

The Engineering Toolbox, 2009. *Air - Thermal Conductivity.* [Online] Available at: https://www.engineeringtoolbox.com/air-properties-viscosity-conductivity-heat-capacity-d_1509.html[Accessed 16 3 2020].

The Engineering Toolbox, 2010. *Water - Heat of Vaporization.* [Online] Available at: https://www.engineeringtoolbox.com/water-properties-d_1573.html[Accessed 5 2 2020].

The Engineering Toolbox, 2018. *Air - Thermal Diffusivity.* [Online] Available at: https://www.engineeringtoolbox.com/air-thermal-diffusivity-d_2011.html [Accessed 16 3 2020].

Warcup, J., 1951. Soil-steaming: A selective method for the isolation of ascomycetes from soil. Trans. Br. Mycol. Soc. 34 (4), 515–518. https://doi.org/10.1016/S0007-1536(51)80035-4.

Welle, A. v. d., 2016. *Ontwerp van elektriciteitsmarkten – benodigde aanpassingen voor een flexibeler energiesysteem op korte termijn.* [Online] Available at: https://repository.tno.nl/islandora/object/uuid%3A2df73fc0-25bf-4a83-a170-1349a66bef9d[Accessed 9 3 2020].

Wikipedia, 2019. *Mass diffusivity.* [Online] Available at: https://en.wikipedia.org/wiki/Mass_diffusivity[Accessed 5 2 2020].

Wikipedia, 2020. *Thermal diffusivity.* [Online] Available at: https://en.wikipedia.org/wiki/Thermal_diffusivity[Accessed 11 3 2020].